

1-1-2009

Prediction Of Particle Laden Flow In Gas Pipe

Mohsen. Hedayati-dezfooli
Ryerson University

Follow this and additional works at: <http://digitalcommons.ryerson.ca/dissertations>

 Part of the [Mechanical Engineering Commons](#)

Recommended Citation

Hedayati-dezfooli, Mohsen., "Prediction Of Particle Laden Flow In Gas Pipe" (2009). *Theses and dissertations*. Paper 1114.

This Thesis is brought to you for free and open access by Digital Commons @ Ryerson. It has been accepted for inclusion in Theses and dissertations by an authorized administrator of Digital Commons @ Ryerson. For more information, please contact bcameron@ryerson.ca.

TJ
935
HE3
2009

PREDICTION OF PARTICLE LADEN FLOW IN GAS PIPE

By

Mohsen Hedayati-dezfooli

B.Eng. Ryerson University, 2008

A Thesis

Presented to Ryerson University

In partial fulfillment of the requirement for the degree of

Master of Applied Science

In the Program of

Mechanical Engineering

Toronto, Ontario, Canada, 2009

© M.H. Dezfooli 2009

PROPERTY OF
RYERSON UNIVERSITY LIBRARY

Author Declaration

I hereby declare that I am the sole author of this thesis or dissertation.

I authorize Ryerson University to lend this thesis or dissertation to other institutions or individuals for the purpose of scholarly research.

I further authorize Ryerson University to reproduce this thesis or dissertation by photocopying or by other means, in total or in part, at the request of other institutions or individuals for the purpose of scholarly research.

ABSTRACT

PREDICTION OF PARTICLE LADEN FLOW IN GAS PIPE

Mohsen Hedayati-dezfooli

Master of Applied Science

Mechanical Engineering, 2009

School of Graduate Studies

Ryerson University, Toronto, Ontario, M5B 2K3, Canada

In the present study, the behavior of various sizes of black powder particulates, carried by a turbulent flow of natural gas, is numerically predicted in a horizontal pipeline. The particles are magnetite and are considered as discrete or a dispersed phase; however, the gas phase is considered as a continuous phase. The numerical approach taken to simulate the dispersed phase is a Lagrangian approach, which is essentially computation of particles trajectories. The turbulence effect on the dispersion of the particles, due to turbulent eddies in the gas phase, is predicted using a stochastic discrete-particle approach. Several case studies have been examined and they include: instantaneous injection of diverse particle sizes, continuous injection of five different particle sizes and multiple injection. For the case with instantaneous injection, it has been found that sudden injection of relatively high mass loading of particles would alter the flow profile in the core region and subsequently increases the turbulent intensity. For all cases it has been found that most particles in the core region of the flow move faster than the gas. Also, for all studied cases, the velocity profiles of gas and particles, at different pipeline stations, have been presented and analyzed.

Borrower

Ryerson University requires the signatures of all persons using or photocopying this thesis.

Please sign below, and give address and date.

ACKNOWLEDGEMENTS

The author would like to sincerely thank Professor Ziad Saghir and Professor Marcello Papini from Ryerson University and Dr. Ehab Elsaadawy from ARAMCO for their helpful assistance, guidance and encouragement throughout the completion of this thesis. Without their help, it was quite impossible for the author to complete this thesis. The author would also like to express his appreciation to his parents Mehdi and Mina for their support. The author also acknowledges the support and useful suggestions of his colleagues Md. Abdur Rahman, M. M. Shemirani and A. Parsa PhD students of Ryerson University.

TABLE OF CONTENTS

Author Declaration.....	ii
Abstract.....	iii
Acknowledgements.....	v
Table of Contents.....	vii
List of Tables.....	x
List of Figures	xi
Nomenclature.....	xiv
CHAPTER 1 – Literature on Black Powder.....	1
1.1 Introduction.....	1
1.2 Characteristics and Formation Sources of Black Powder.....	2
1.3 Movement of Black Powder in Gas Pipeline.....	6
1.4 Gas-Particle Flow.....	10
1.4.1 Literature.....	10
1.5 Literature Survey Summary.....	14
CHAPTER 2 – Mathematical Formulation & Numerical Approach.....	17
2.1 Introduction.....	17

2.2 Equations of Motion for Particles.....	17
2.2.1 Particle Force Balance.....	17
2.2.2 Stochastic Particle Tracking in Turbulent Flow.....	19
2.2.3 Integration of the Trajectory Equation.....	20
2.3 Coupling between the Discrete and Continuous Phases.....	21
2.3.1 Momentum Exchange.....	21
2.4 Modeling Turbulence.....	22
2.4.1 Transport Equations for the Standard k- ϵ Model.....	22
2.5 Continuity and Momentum Equations.....	24
2.5.1 Continuity Equation.....	24
2.5.2 Momentum Conservation Equations.....	24
CHAPTER 3 – Turbulent Gas Flow in Horizontal Pipe.....	27
3.1 Introduction.....	27
3.2 Mesh Consideration and Validation of the Model near the Pipe Wall.....	31
3.2.1 The Law of Wall.....	31
3.2.2 Evaluation of Friction Coefficient.....	34
3.3 Gas Flow Velocity.....	35
3.3.1 Validation of Gas Flow Velocity Profile.....	39
3.4 Turbulent Intensity.....	40

CHAPTER 4 – Particle Laden Flow Modeling in Horizontal Gas Pipeline.....	45
4.1 Introduction.....	45
4.2 Validation of the Model Approach.....	48
4.3 Results Analysis.....	50
4.3.1 Instantaneous Injection of Diverse Particle Sizes	50
4.3.2 Continuous Injection of 25 μm Particles.....	60
4.3.3 Continuous Injection of 10 and 50 μm Particles.....	67
4.3.4 Continuous Injection of 75 and 150 μm Particles.....	71
4.3.5 Multiple Injections with Maximum Gas Volume Flow Rate.....	74
CHAPTER 5 – Conclusion and Future Work.....	79
APPENDIX – Input File for CFD Model Setup.....	80
A.1 Instantaneous Injection of Diverse Particle Sizes- Case Study.....	80
A.2 Continuous Injection of 10, 25, 50, 75 and 150 μm Particles- Case Study.....	82
A.3 Multiple Injections with Maximum Gas Volume Flow Rate- Case Study.....	85
REFERENCES.....	89

LIST OF TABLES

Table 3.1 Properties of sales gas at 288 °Kelvin.....	29
Table 3.2 Gas flow characteristics at the inlet at operating conditions.....	29
Table 3.3 Characteristics of the pipe.....	29
Table 3.4 Boundary conditions.....	30
Table 4.1 Characteristics of the pipe.....	48
Table 4.2 Particle properties.....	51
Table 4.3 Particle injection setup.....	51
Table 4.4 Characteristics of the gas flow at the inlet at operating conditions.....	52
Table 4.5 CFD model boundary condition setup.....	52
Table 4.6 Particle properties.....	62
Table 4.7 Particle injection setup.....	62
Table 4.8 Characteristics of the gas flow at the inlet at operating condition.....	63
Table 4.9 CFD model boundary condition setup.....	63
Table 4.10 Particles size and mass flow rate.....	75

LIST OF FIGURES

Figure 1.1 SEM of black powder particulates.....	2
Figure 1.2 Required gases velocity to move minerals.....	8
Figure 1.3 Required minimum velocities.....	8
Figure 1.4 Required velocity as function of particle size.....	9
Figure 1.5 Required flow rates to move one μm particle at various pipe pressures.....	9
Figure 3.1 Schematic of turbulent flow development in pipe.....	28
Figure 3.2 Velocity profile distribution in turbulent flow near the wall.....	33
Figure 3.3 y^+ Plot at the wall.....	33
Figure 3.4 Variation of the skin friction coefficient along the axial length of the pipe	35
Figure 3.5 Axial velocities along the centerline vs. axial distance.....	37
Figure 3.6 Radial variations of velocity vs. various pipeline stations.....	39
Figure 3.7 Illustration of RMS & velocity fluctuation data about a mean value of velocity.....	41
Figure 3.8 Turbulent intensity vs. axial distance.....	42
Figure 3.9 Radial variations of turbulent intensities vs. various pipeline stations.....	43

Figure 4.1 Various mesh sensitivities of mean air velocity distribution with zero particle mass loading for bulk air velocity of 10.6m/s	49
Figure 4.2 Comparison of our results with results obtained by C.K.K Lun [35] for particle mass loading of 0.5.....	49
Figure 4.3 Gas velocity profile at the inlet and outlet of the pipe before particle injection.....	53
Figure 4.4 Graphical tracking of black powders particulates, carried by fully developed gas flow, from injection point to the outlet within 4 seconds from (a) to (h).....	54
Figure 4.5 Graphical tracking of black powders particulates, carried by fully developed gas flow, from injection point to the outlet within 4 seconds from (a) to (e).....	56
Figure 4.6 Velocity profile of the gas just before and 4 seconds after injection of particles at every segment of pipeline from injection point to the outlet.....	57
Figure 4.7 Stream wise turbulent intensity profile of gas before and within 4 seconds of particle injection. The values at each time are correspondent to every segment of pipeline from injection point to the outlets.....	58
Figure 4.8 Velocity profile of the gas and particles at the outlet 4 s after injection	59
Figure 4.9 Distribution of particles size at the outlet vs. particles radial distance from pipe bed.....	59
Figure 4.10 Graphical tracking of black powders particulates, carried by fully developed gas flow, from injection point to the outlet.....	64
Figure 4.11 Graphical tracking of black powders, colored by particle residence time.....	64
Figure 4.12 Velocity profile of gas at inlet and outlet during particle injection.....	65
Figure 4.13 Velocity profiles of gas and 25µm particles at the pipeline outlet.....	65
Figure 4.14 Stream wise turbulent intensity profile of gas at the inlet, middle and outlet of the pipeline.....	66

Figure 4.15 Concentration of particles along the pipeline bed in terms of particles mass per unit volume.....	66
Figure 4.16 Graphical tracking of black powders particulates, carried by fully developed gas flow, from injection point to the outlet for (a) particles with diameters of 10 μm and (b) particles with diameters of 50 μm	68
Figure 4.17 Velocity profiles of gas and particles at the pipeline outlet.....	69
Figure 4.18 Velocity profiles of gas and particles at the pipeline middle.....	69
Figure 4.19 Concentration of particles along the pipeline bed in terms of particles mass per unit volume.....	70
Figure 4.20 Graphical tracking of black powders particulates, carried by fully developed gas flow, from injection point to the outlet for (a) particles with diameters of 75 μm and (b) particles with diameters of 150 μm	72
Figure 4.21 Velocity profiles of gas and particles at axial distance of 6.5m from the injection point.....	72
Figure 4.22 Concentration of particles along the pipeline bed in terms of particles mass per unit volume.....	73
Figure 4.23 Graphical tracking of multiple injections of black powders particulates, carried by fully developed gas flow, from injection point to the outlet for different size particles.....	75
Figure 4.24 Velocity profiles of gas and particles at the pipeline outlet.....	76
Figure 4.25 Velocity profiles of gas and particles at the pipeline middle.....	76
Figure 4.26 Velocity magnitudes of particles at the outlet vs. particles angle of orientation.....	78
Figure 4.27 Radial distance of particles at the outlet vs. particles angle of orientation.....	78

NOMENCLATURE

u_p	Particle velocity (m/s)
u	Instantaneous gas phase velocity (m/s)
u'	Instantaneous gas velocity fluctuations (m/s)
\bar{u}	Mean gas velocity (m/s)
u'_p	Instantaneous particle velocity fluctuation (m/s)
u	Velocity of gas as function of density, viscosity, wall shear stress and thickness
u_c	Gas velocity at core region (m/s)
g	Gravitational acceleration (m/s^2)
F_D	Drag Force (N)
F	Other Forces (N/Kg)
μ	Gas viscosity (Kg/m-s)
ρ	Gas density (Kg/m^3)
ρ_p	Particle density (Kg/m^3)
d_p	Particle diameter (m)
Re	Reynolds number (dimensionless)
C_D	Drag coefficient (dimensionless)
t	Time (s)
τ_p	Relaxation time of particle (s)

Δt	Time step (s)
\dot{m}_p	Mass flow rate of particle (Kg/s)
k	Turbulent kinetic energy (J/kg)
ε	Turbulent dissipation rate (m^2/s^3)
μ_t	Turbulent viscosity (Kg/m-s)
M_t	Mach number (dimensionless)
S_m	Mass source (Kg)
P	Static pressure (psi)
F_x	External body forces in axial direction (N)
F_y	Gravitational body force in radial direction (N)
T	Temperature (Kelvin)
C_p	Specific heat (J/Kg-Kelvin)
ϵ	Wall roughness of pipe (m)
d	Pipe diameter (m)
f	Coefficient of friction (dimensionless)
R	Pipe radius (m)
R	Gas-Law constant (8.31447 J/Kg-mol-K)
V	Gas volume (m^3)
P	Momentum transfer rate (Kg-m/s ²)

CHAPTER 1

Literature on Black Powder

1.1 Introduction

The term black powder refers to different forms of iron sulfide, iron oxide and carbonates mixed with contaminants. It is the most well known contaminant in natural gas pipelines and compression equipment in pipeline, refinery, gathering, and storage applications. However, in some cases, there may be only one form present. For instance, in the case of Saudi Aramco (Oil Company), iron oxide (Magnetite- Fe_3O_4) and iron hydroxides (Fe-OOH) are the main components with no iron sulfides present. Black powder is an important operating problem in wet and dry gas pipelines. It represents a threat to pipeline operation and natural gas's reputation as a clean fuel. It is a worldwide phenomenon experienced by most, if not all, gas pipeline operators. For many years, pipeline companies have observed its presence and effects but have viewed it only as an annoyance. They have devoted almost no attention to assessing the costs of the problem. The occurrence of black powder is causing increasing concern in the natural gas industry worldwide. Although it is a relatively new phenomenon, a growing number of pipeline operators are now turning their attention to the problem, because of the substantial effects it has on their pipeline systems. In combination, these effects and the wide range of other difficulties are creating a major challenge for pipeline operators (notably for pigging activities such as cleaning and inspection). Black powder clogs instruments and reduces the overall gas flow through the pipes. This chapter will present the characteristics and the nature of black powder, its sources, formation mechanisms, its movement in gas pipelines and literature on gas particle flow.

1.2 Characteristics and Formation Sources of Black Powder

In the gas industry, the term “black powder” is a color-descriptive term loosely used to describe a blackish material that collects in gas pipelines leading to erosion failures of valves, lowering efficiency for compressors, clogging of instrumentation and customer complaints [1-5]. Formation cuttings, drilling mud, desiccant dust, construction dirt, sand, mill scale, iron oxide, iron carbonate, iron sulphide, welding slag and splatter, eroded steel cuttings, salt crystals, valve-grease, corrosion inhibitor and other organic materials can all contribute to the presence of black powder [6]. According to the study of Villea et al. [7], the range of black powder particle size indicates that in the same pipeline we can find various sizes of particles. For instance, dividing this range into different samples in a certain natural gas pipeline, sample A with the particles between 210 μm and 44 μm and sample B with the major fraction less than 37 μm can be found. Figure 1.1 shows scanning electron microscope (SEM) photomicrographs of black powder particulates having the size of about 100 μm and smaller [8].

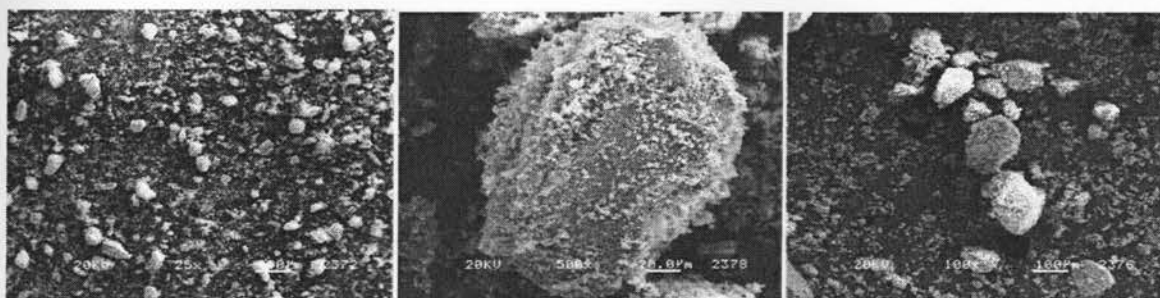


Figure 1.1 SEM of black powder particulates [8]

Generally, black powder is considered a substance composed mainly of iron sulfide and iron oxide, which is a major concern for the natural gas industry because it can cause corrosion and creates wear on pipelines [1]. Black powder may be wet and have a tar-like appearance or dry

and be a very fine powder, sometimes like smoke. It could also be mechanically mixed or chemically combined with any number of contaminants such as salts, sand, liquid hydrocarbons, and metal debris [9]. According to Abdelmounam studies [9], different gas pipeline operators report different compositions for black powder removed from their pipelines. For example, whereas some literature reports black powder as being predominantly iron sulfides [1-3], others report the complete absence of iron sulfides but the presence of iron oxide such as Fe_3O_4 and $FeOOH$ [4,10]. On the other hand, others report a combination of all of these products (iron sulfide, iron carbonates and iron oxides) [5]. However, all these products have one common source which is the natural gas pipeline. In fact, they are all being formed in natural gas pipelines as a result of corrosion of the internal walls of the pipeline [1-5] & [10] and more specifically, by reaction of iron (Fe) presented in ferrous steel pipeline with condensed moisture containing oxygen (O_2), hydrogen sulfide (H_2S) and carbon dioxide (CO_2). All these products are relatively high in specific gravity (sp. gr. 4 to 5.1), abrasive and typically difficult to remove in cleaning operations [5]. Case histories showed that large quantities of black powder can be generated inside pipelines. For instance, 3628 Kg of black powder have been removed from a 16 inch by 80 km pipeline in Houston and 500 kg from a 36 inch x12 km Greek Sales Gas transmission pipeline [4]. Internal corrosion in "dry" gas pipelines is often ignored due to an underestimation of the corrosion risk due to a seeming absence of condensed water in the pipeline [1-5] & [11]. Under normal conditions, a gas pipeline are under minimal corrosion risk; however, it is not possible to completely eliminate water from pipelines [11]. Water vapor can potentially condense at the inner wall of the pipeline due to high dew points. Water vapor can also enter the pipeline through periodic upsets that cause water carry-over into the line. This water, coupled with corrosive species such as CO_2 , H_2S and O_2 in small amounts (ppm), can result in

unexpected internal corrosion of the inner pipe wall and form products such as FeCO_3 , FeS and iron oxides/hydroxides [1-5]. It should be noted that these components also exist in dry gas naturally and form weak acid that can cause significant corrosion [1]. Carbon dioxide is a naturally occurring constituent of natural gas; this is in contrast with oxygen gas which could penetrate through leaks at low pressure points throughout the pipeline systems [1]. Oxygen in gas pipelines can cause significant corrosion in small concentrations and even combustion in larger amounts. According to Craig [12], a 1988 survey of 44 natural gas transmission pipeline companies in North America indicate that their gas quality specifications allowed maximum O_2 concentrations ranging from 0.01 mol% to 0.1 mol% with typical value of 0.02% mol. It has been shown that oxygen content of approximately 0.01 mol % has little effect on steel corrosion in the presence of stagnant water inside sales gas transmissions while 0.1 mol% produces fairly high corrosion rates. Therefore, as a general rule, it has been recommended that transmission pipeline operators should consider limiting maximum oxygen concentrations to 10 ppmv (part per million volumes) which is 0.01 mol%. According to the study of Baldwin [1], hydrogen sulfide can also be a naturally occurring constituent of natural gas or alternatively produced by sulfate reducing bacteria (SRBs). These anaerobic bacteria use the reduction of sulfate as source of energy and oxygen, in accordance with reactions such as:

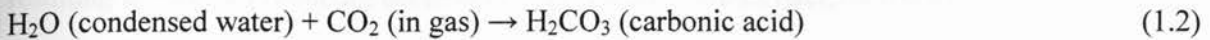


Since condensed water is a prerequisite for these bacteria to activate, such a reactions cannot occur in the absence of water. Therefore, typical Sales Gas standards specify a maximum moisture content limit of 7 lbs water/mmscf (Million Standard Cubic Feet) which is about 0.112 mg/liter. Corrosion processes due to H_2S , CO_2 and O_2 in sales gas pipelines have well established

mechanisms. According to the study of Craig [12] and Baldwin [1], electrochemical reactions that describe these corrosion processes and their respective corrosion products are presented as:

FeCO₃ formation due to CO₂ corrosion:

The source of siderite-FeCO₃ corrosion products is the chemical reaction of dissolved CO₂ in condensed water producing carbonic acid which in turn reacts directly with steel to produce FeCO₃, in accordance with these reactions:



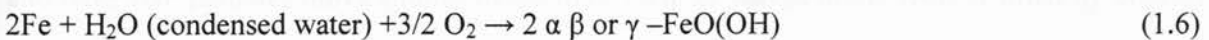
Iron Sulfide formation due to H₂S corrosion:

Iron sulfide (FeS) corrosion products are usually formed from H₂S, naturally occurring in natural gas or produced by SRB (sulfate reducing bacteria), reacting directly with the steel wall of the pipeline as per the following reactions:



Iron oxides formation due to oxidation:

In cyclical wet-dry low dissolved oxygen environments, iron oxides are usually formed by the direct oxidation of pipeline steel walls, in accordance with the following reactions:



In water containing low concentrations of dissolved oxygen, as is the case in the sales gas environment, the γ -Fe(OH) is unstable and will quickly transform to magnetite-Fe₃O₄ and water by the following reaction:



But if the water is nearly saturated with dissolved oxygen, then hematite (Fe₂O₃) is often present. Alternatively, iron oxides may be formed due to microbiologically induced corrosion (MIC) resulting from acid producing bacteria (APB) or iron oxidizes bacteria (IOB).

1.3 Movement of Black Powder in Gas Pipeline

Black powder movement in a pipeline is as important as its presence since it can move through a pipeline carried by the gas velocity. According to Smart [14], when black powder is transported through the pipeline by the gas flow, the velocity required to move dry solids in a pipeline can be calculated and depends on pipeline diameter, gas pressure, density, viscosity and particle size and density. For instance, typical velocities required at 1000 psi are 10 ft/sec for 8-inch pipelines, 13 ft/sec in 24-inch pipelines and 14 ft/sec in 48-inch pipelines. Operators report that when black powder moves, it shatters and becomes very small in size, in the range of one micron (μm) or less, making it difficult to filter and possibly easier to move. Once black powder starts to move, it will continue to move until the flow rate is reduced or the gas is compressed. The nature of particle motion depends not only on gravity, but also on particle shape. For instance rounded particles roll, long thin particles slide, irregularly shaped particles move in a series of bounces, and flake-like particles move similar to the movement of leaves in the wind if lifted by viscous forces [13]. Deposition of black powder will occur if the velocity is not high enough to drag the

particles along by viscous flow forces. Sediment deposits can lead to blockage of the line, especially during pigging. In addition, flowing powder can damage compressors, plug filters and damage equipments. Engineers and operators have advised that they consider a pipeline clean when the friction factor is less than a certain value, solids are not evident in the receiving pig trap ahead of a pig and a bare foam pig run through the line has less than ½ inch penetration of dirt into the foam. According to Smart's studies [14], solid particles in a gas pipeline will move when the gas velocity causes enough drag force on a particle to push it along. If black powder exists as a crusted or wet deposit, pigging can scrape the powder and enable it to move; however, a much greater velocity is required. From Smart's study, it was found that each particle in gas pipeline is affected by forces such as gravity, buoyancy, lift and drag. Gravity and buoyancy are constant, while lift and drag vary with flow conditions, depending on inertia and viscosity of the gas. At low flow rates, gravity and buoyancy predominate and particles settle to the bottom to form a layer of sediment. The sediment layer continues to grow until the velocity in the remaining cross-sectional area is great enough to move the particles along. Wicks [15] developed a technique to calculate the velocity required to sweep dry solids through horizontal pipelines by fluid drag. The technique was developed to predict the fluid velocity at which particles could be pulled up from a bed of particles in the bottom sides of a pipeline and then carried through the pipeline. Wicks [15] derived two expressions containing the hydrodynamic parameters affecting a particle:

$$\Psi = [\rho_f^3 d V^4] / [(\rho_p - \rho_f) g_L \mu^2] \quad (1.8)$$

$$S = [D_{eq} V_s \rho_f (d/D_p)^{2/3}] / \mu \quad (1.9)$$

where ρ_f is fluid density, ρ_p is particle density, d is the weight average particle diameter, V is the average flow velocity in the area above a bed, g is gravitational acceleration, μ is fluid viscosity, D_{eq} is equivalent diameter of the flow region above the particle bed and D_p is inside pipe diameter. Wicks [15] found that the two parameters are related by:

$$\Psi = S^3 / (10 + 0.01S^{3/2}) \quad (1.10)$$

Note that the above correlation can be solved only by trial and error. Wick's correlation was applied in order to acquire the prediction of required gas velocities to move black powder particulates in gas pipelines under various conditions. Figure 1.2 [14], shows the required velocities to move various black powders' constituents in a 24 inch horizontal pipe. The specific gravity is considered as 0.63 and a pressure of 1000 psi at the temperature of 60°F or 15.5°C. Figure 1.3 [14] shows, for different pipeline diameters and pressures, what minimum velocity is required to move 1 μm of Iron Sulfide and Iron Oxide (magnetite) in a pipeline.

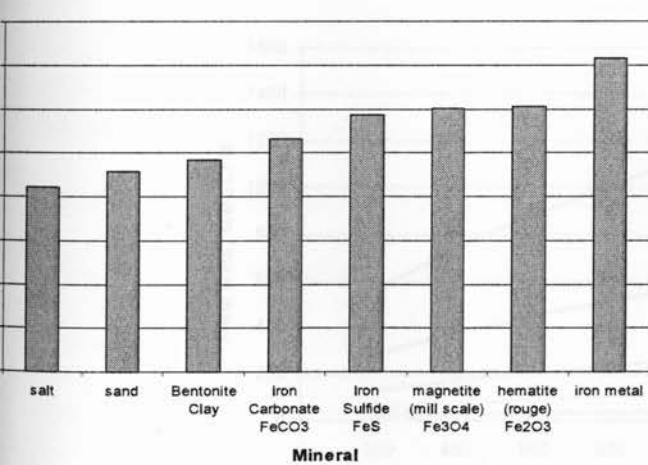


Figure 1.2 Required gases velocity to move minerals [14]

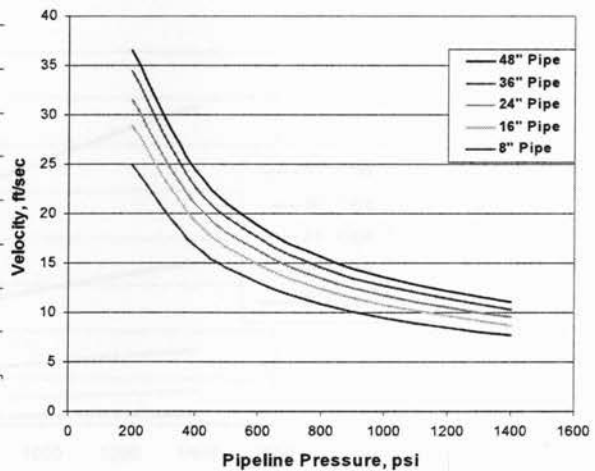


Figure 1.3 Required minimum velocities [14]

Figure 1.4 [14] illustrates the effect of particle size on velocity requirements to move the particle for 8, 16, 24, 36 and 48 inch of the gas pipeline diameters.

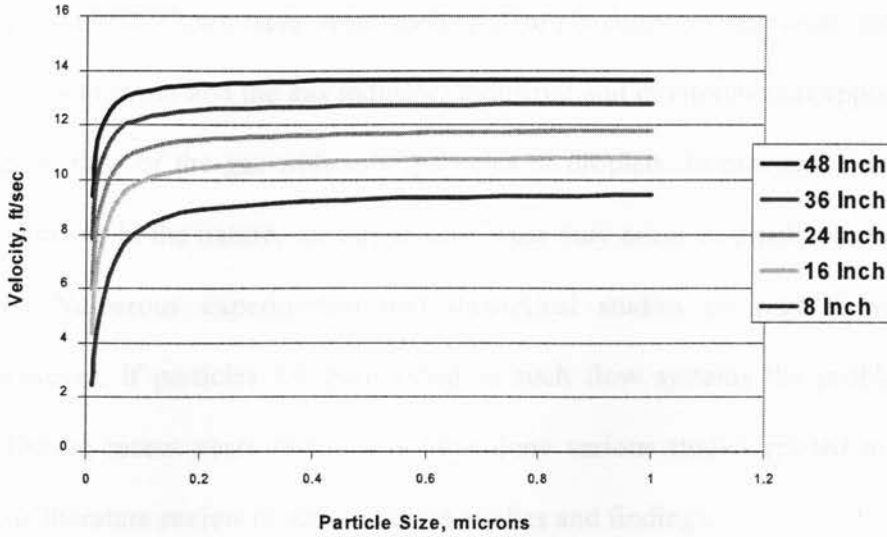


Figure 1.4 Required velocity as function of particle size [14]

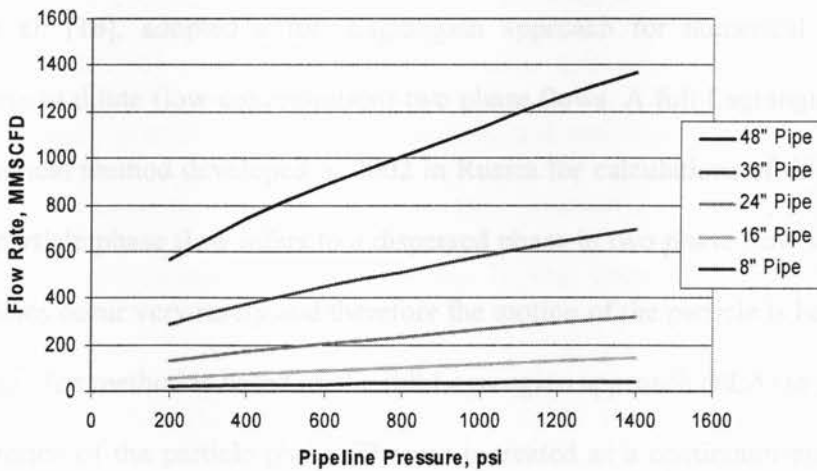


Figure 1.5 Required flow rates to move 1 μm particle at various pipeline pressures [14]

Figure 1.5 [14] illustrates required flow rates in scale of mmscfd (million standard cubic feet per day of gas) to move 1 μm of black powder particle for different pipeline pressures and diameters.

1.4 Gas-Particle Flow

Two phase gas-particle flows have wide industrial applications in chemical process plants, thermal power engineering and the gas industry. Industrial and environmental applications often involve turbulent flow of the gas with solid particles or droplets. In practical situations where particles are abrasive in the nature, serious erosive wear may occur in pipelines conveying gas-particle flows. Numerous experimental and theoretical studies on pipe flow have been performed; however, if particles are transported in such flow systems the problem becomes challenging. During recent years researchers have done various studies related to gas-particle flows. Below is literature review of some of these studies and findings.

1.4.1 Literature

Tsirkunov et al. [16], adopted a full Lagrangian approach for numerical treatment of the dispersed phase in dilute (low concentration) two phase flows. A full Lagrangian approach is an efficient numerical method developed in 2002 in Russia for calculations of dilute particle phase flow. Dilute particle phase flow refers to a dispersed phase in two phase flow system if collision between particles occur very rarely and therefore the motion of the particle is being controlled by the fluid forces. The method is based on the full Lagrangian approach (FLA) to the description of the regular motion of the particle phase. The gas is treated as a continuum phase for which all basic equations, namely, the continuity equation, the momentum equations and the energy equation are written in the Lagrangian coordinates. The main difference between this approach

and the traditional Lagrangian approach is that in the traditional approach the explicit form of the continuity equation for the particle phase is not considered; however, in a full Lagrangian approach this is considered. In addition, in a full Lagrangian approach you would also find numerical calculations of two-phase flows with a “complex” particle phase flow structure. According to Crowe et al. [17], the description of a ‘dilute’ particle phase flow in Lagrangian coordinates is very convenient compared with an Eulerian approach because the momentum, angular momentum and thermal energy equations are in terms of ordinary differential equations when using the Lagrangian approach, whereas they have the form of partial differential equations when using the Eulerian approach. However, Tsirkunov et al. [16] described the carrier gas flow in Eulerian coordinates when the volume fraction of the discrete phase is not negligible. In fact the Eulerian approach is more suitable and beneficial when dealing with gas flow fields with a considerable volume fraction of particle phase.

Sommerfeld [18], introduced inter-particle and wall particle collision effects in the frame of the Lagrangian approach for the particle phase. Sommerfeld analyzed the behavior of spherical solid particles in a horizontal channel flow by applying numerical calculations based on the Lagrangian approach by considering particle motion, wall collisions, wall roughness, and inter-particle collisions. Sommerfeld discussed the particle behavior for different conditions, such as particle size, wall roughness and mass loading. It was demonstrated that effects of wall roughness and inter-particle collisions have a dramatic influence on the particle behavior in a horizontal channel and the particle phase properties of the developed flow. Also Sommerfeld introduced the mean free path between wall collisions to characterize the behavior of particles and it was demonstrated that for small particles, wall roughness causes a considerable reduction of wall collision frequency meaning that the wall collision mean free path increases.

According to Sommerfeld [18], wall roughness has a significant effect on the horizontal particle mean velocity and the fluctuating components. Indeed, depending on the degree of roughness, the particle mean velocity is reduced, while the fluctuating velocities are considerably increased. It was also demonstrated that for small particles the wall collision frequency reduces with increasing mass loading for smooth and rough walls as a result of inter-particle collisions. For this reason the possibility of particle degradation might be reduced during wall impact and pressure loss. In contrast, when dealing with the case of larger particles, wall roughness impact is dominating and a smooth wall will yield lower wall collision frequencies, resulting also in lower pressure drop.

Lun and Liu [19] developed a model of a dilute turbulent gas-solid two phase flow using a set of conservation equations for mass and momentum, and a two-equation $k-\varepsilon$ closure. They determined the trajectories and velocities of the solid particles by integrating the particle equation of motion using the Lagrangian approach. Their results for two phase flow showed that inter-particle collision plays an important role to maintain fully developed and steady suspension of the particles. The simulation of the results agreed with the experimental data for the averaged gas velocity, averaged particle velocity and its concentration and pressure gradient of fluid. They also presented macroscopic velocities, air turbulence intensity, granular temperatures, angular momentum fluxes and particle stresses.

Vance et al. [20] investigated spatial characteristics of the particle velocity field using numerical simulations of gas-solid turbulent channel flow. They adopted incompressible Navier-Stokes equations to solve for the gas phase and computed particle phase by using the Lagrangian method considering that the particle's motion is governed by the drag force. They measured the particle velocity field in planes parallel to the wall.

Durst et al. [21] introduced two approaches to predict particulate two-phase flows. In the first approach (Lagrangian) the fluid phase is considered a continuum phase and the particulate phase in the fluid as a discrete phase. In the second approach (Eulerian) the particulate phase is considered as continuum phase. Their study showed that Lagrangian approach has some advantages for predicting particle flows in which large particle accelerations occur. However, the Eulerian approach seems to have advantages in flow cases where high particle concentrations occur.

Keska [22] conducted some experimental research for solid-gas flow in a horizontal pipe using the capacitive technique for measurements of flow velocity and spatial concentration. The system of measurement was developed to detect the transients in the flow regimes in the dilute and dense phases. In Keska's view, phase velocity and spatial concentration are the most fundamental parameters in the study of solid-gas flow. Indeed, in gas-solid flow regimes, transients are manifested as a change of spatial concentration and distribution in time and space and produce oscillation. Hence, these oscillations cause mechanical vibrations and erosion of the system components and generate pressure waves with specific frequencies.

Henein et al. [23] conducted an experimental study to investigate the phenomenon of powder injection into a turbulent gas stream flowing in a cylindrical pipe. The experiment focused on the radial dispersion of particles. Their findings have shown that the particle size and density have important effect on radial dispersion of particles in a pipe. For instance, 70 μm silica particles have shorter dispersion lengths in comparison with 1 μm fog particles. It was also found that the presence and projection of the injector into the turbulent flow causes a larger turbulent intensity than without its presence in the flow stream. Indeed, dispersion length of fog droplets decreases with increasing injector protrusion. Moreover, their studies on the forces acting on the particles

injected into the turbulent stream show that radial Reynolds stress is the primary mechanism for the radial dispersion of particles in pipe flow. Radial dispersion into the turbulent stream is attributed to the radial forces such as forces due to the velocity gradient in the radial direction, radial pressure gradient, radial Brownian motion and radial turbulent shear force.

Daniel et al. [24] experimentally studied the response of glass particles in a fully developed turbulent channel flow of humidified air. The mass loading of particle to air volume was on the order of 10%. In their experiments, laser sheets were aligned in stream-wise flow planes, so the particle-laden flow could be imaged with a dual-frame camera. They added a small amount of fog particles (glycerin droplets 1-3 μm) to the flow at the entrance in order to provide a means for measuring gas velocity. Sets of five different sizes of solid spheres were examined. It was found that larger particles (e.g. 100-160 μm) moved faster than the gas near the wall. For small particles (e.g. 20-30 μm), drift velocity is significant close to the wall so that smaller particles tended to reside in the low speed stream; however, near the center-plane drift velocities were found to be very small for all particle sizes. At the center-plane it was shown that larger particles move slower than gas (note that Reynolds number is 4500). This was in comparison with Kulick et al.'s [25] experimental results with Reynolds of about 13800 in which shows that particles move always faster than gas at the channel center-plane.

1.5 Literature Survey Summary

Based on above literature survey as well as data from ARAMCO, we can summarize a few concluding remarks which will be considered in the following chapters. Regarding the kind of black powder particulate, in this study, we may consider iron oxide (Magnetite- Fe_3O_4) which has density of 5150 Kg/m^3 with sizes ranging from 1 to 150 μm . The diameter of the pipe model

would be selected as standard 40 inch sales gas pipeline which has roughness of 30 μm . According to the studies of Smart [14] and Wicks [15] and with respect to the diameter of the pipe and characteristics of black powder particles the required gas flow velocity to be considered in this study can be estimated as about 6 to 8 m/s. Also, simulation of the results should be implemented at an operating pressure of about 900 psi (Figure. 1.5). Finally, the approach chosen in this study would be the Lagrangian approach since the fundamental basis in this study is similar to work done by Lun and Liu [19].

CHAPTER 2

Mathematical Formulation and Numerical Approach

2.1 Introduction

In this study the numerical approach taken to simulate the behavior of the particles as a discrete second phase is the Lagrangian approach, which is essentially computation of particles trajectories. This is in addition to solving transport equations for the gas as a continuous phase. Computation of discrete phase trajectory using a Lagrangian formulation includes the discrete phase inertia, the hydrodynamic drag, and the force of gravity for both steady and unsteady flows. Also, the turbulence effect on dispersion of particles due to turbulent eddies in the gas phase is predicted using a stochastic discrete-particle approach. Basically, in the stochastic tracking approach, the turbulent dispersion of particles is being predicted by integrating the trajectory equations for every particle using the instantaneous gas velocity along the particle path. In the following subsections the mathematical formulation to solve the gas-particle flow is presented. All the equations and related comments in this chapter are directly referenced from the FLUENT user manual documentation.

2.2 Equations of Motion for Particles

2.2.1 Particle Force Balance

The trajectory of particles is being predicted by integrating the force balance on individual particles. The force balance represents equating the forces acting on particles and particles inertia in the axial direction of Cartesian coordinates:

$$\frac{du_p}{dt} = F_D(u - u_p) + \frac{g(\rho_p - \rho)}{\rho_p} + F \quad (2.1)$$

where $F_D(u - u_p)$ represents the drag force per unit particle mass, u is gas phase velocity, u_p is particle velocity and g is gravitational acceleration. F_D can be defined as

$$F_D = \frac{18\mu}{\rho_p d_p^2} \frac{C_D R_e}{24} \quad (2.2)$$

where μ, ρ, ρ_p, d_p respectively denote gas viscosity, gas density, particle density and particle diameter. R_e denotes relative Reynolds number where can be defined as

$$R_e = \frac{\rho d_p |u_p - u|}{\mu} \quad (2.3)$$

C_D , the drag coefficient, can be computed from following equation

$$C_D = a_1 + \frac{a_2}{R_e} + \frac{a_3}{R_e^2} \quad (2.4)$$

a_1, a_2 and a_3 are constants applied for spherical particles.

The term F , incorporated in equation (2.1), denotes additional forces per unit particle mass that may be considered in the particle force balance depending on circumstances. These forces are as follows; virtual mass forces, forces in rotating reference frames, thermophoretic forces, Brownian forces and Saffman's lift forces. Forces in rotating reference frames include forces on particles that arise due to rotation of the reference frame. Thermophoretic force is a phenomenon where small particles, suspended in a gas with a temperature gradient, experience a force in the opposite direction to that of the gradient. The Brownian force is a force that should be considered

when dealing with very small particles in the range of sub-micron. The Virtual mass force is the force required to accelerate the fluid surrounding the particle and should be considered only when the density of the fluid is greater than that of the particle, which is not the case in this study. Finally, Saffman's lift force, or lift due to shear, is only valid for sub-micron particles. Since none of above forces is applicable in this study it can be concluded that the term F has a value of zero in equation (2.1).

2.2.2 Stochastic Particle Tracking in Turbulent Flow

When the flow is turbulent the prediction of trajectories of particles can be implemented using the mean gas velocity, denoted by \bar{u} , as well as its instantaneous velocity fluctuations, denoted by u' . The summation of these two represents instantaneous gas velocity, u along the particle path as shown below:

$$u = \bar{u} + u'(t) \quad (2.5)$$

By computing the trajectory for an adequate number of particles, (so-called “number of tries”) the random effects of turbulence on the particle dispersion can be determined. The prediction of particle dispersion in a continuous gas flow makes use of the concept of the integral time scale, denoted by T_t . Indeed the integral time scale describes the time spent in turbulent motion along the particle trajectory, d_s which is given by:

$$T_t = \int_0^\infty \frac{u'_p(t)u'_p(t+s)}{u_p'^2} d_s \quad (2.6)$$

where u'_p denote instantaneous particle velocity fluctuation. As shown by equation (2.6), the rate of particle dispersion is directly proportional to integral time, so basically larger values of the integral time indicate greater turbulent motion in gas-particle flows.

2.2.3 Integration of the Trajectory Equation

The trajectory equation is solved by stepwise integration over discrete time steps. The velocity of particles along the particle path at every point can be computed by integrating equation (2.1) with time. This trajectory is predicted by

$$\frac{dx}{dt} = u_p \quad (2.7)$$

Hence, the particles trajectories are predicted by solving equations (2.1) and (2.7) in each coordinate direction. Assuming that all forces in equation (2.1) are linearly acting on particles and they remain constant over every time interval, the trajectory equation can be rewritten as

$$\frac{du_p}{dt} = \frac{1}{\tau_p} (u - u_p) \quad (2.8)$$

where τ_p stands for the relaxation time of the particle. The equation (2.8) is integrated via the trapezoidal rule:

$$\frac{u_p^{n+1} - u_p^n}{\Delta t} = \frac{1}{\tau_p} (u^* - u_p^{n+1}) + \dots \quad (2.9)$$

The trapezoidal rule, in mathematics, is a technique used to approximately calculate the definite integral $(\int_a^b f(x)dx)$. The trapezoidal rule works by approximating the region under the graph of the function $f(x)$ as a trapezoid and calculating its area [Wikipedia, Trapezoidal rule].

where n represents the number of iterations and

$$u^* = \frac{1}{2}(u^n + u^{n+1}) \quad (2.10)$$

$$u^{n+1} = u^n + \Delta t u_p^n \cdot \nabla u^n \text{ or } u^{n+1} = u^n + \Delta t u_p^n \cdot (\partial/\partial x + \partial/\partial y)u^n \quad (2.11)$$

2.3 Coupling between the Discrete and Continuous Phases

While the continuous phase always impacts the particle phase, it is also affected by particle phase trajectories. This two-way phenomenon is called coupling or inter-phase exchange and is incorporated in particle-gas calculations via alternately solving the particles trajectories and the gas phase equations until the solutions in both phases have stopped changing. This inter-phase exchange between the continuous and the discrete phases includes momentum and heat lost or gained by the particle phase stream following the trajectory that is computed. The quantities of these changes will then be incorporated in the subsequent continuous phase computations. Since in this study the effect of heat is not considered, only mathematical formulations for momentum exchange will be discussed.

2.3.1 Momentum Exchange

As particle pass through each control volume, its momentum changes. Each control volume refers to the corresponding cubic node in the CFD model, so depending on the number of nodes

which form the main structure of the model (circular pipe in our case), the number of control volumes varies. The momentum transfer from gas phase to discrete phase can be computed by analyzing the momentum change over a certain time Δt and can be computed by:

$$P = \sum \left(\frac{18\mu C_D Re}{\rho_p d_p^2 24} (u_p - u) + F_{other} \right) \dot{m}_p \Delta t \quad (2.12)$$

where \dot{m}_p denotes the mass flow rate of particles, P denotes momentum transfer rate, F_{other} stands for other interaction forces per unit particle mass and Δt denotes time step.

2.4 Modeling Turbulence

There is no turbulence model that is able to solve all classes of turbulent flows. Indeed to choose an appropriate turbulence model various parameters should be considered such as physical properties of the problem, time availability, availability of computational resources and so forth. In this study, based on the generality of the problem, the methodology selected to solve the turbulent gas flow was chosen to be the standard k - ε model. The standard k - ε model is a semi-empirical model based on transport equations that consist of two differential equations which are transport equations for turbulent kinetic energy k and for turbulent dissipation ε (also referred as viscous dissipation rate). These two equations are solved along with the time-averaged continuity and momentum equations.

2.4.1 Transport Equations for the Standard k - ε Model

The turbulent kinetic energy, k , can be computed from the following transport equation:

$$\frac{\partial}{\partial t} (\rho k) + \frac{\partial}{\partial x_i} (\rho k u_i) = \frac{\partial}{\partial x_j} \left[\left(\mu + \frac{\mu_t}{\sigma_k} \right) \frac{\partial k}{\partial x_j} \right] + G_k - \rho \varepsilon - Y_M \quad (2.13)$$

The turbulent dissipation rate, ε , can be computed from the following transport equation:

$$\frac{\partial}{\partial t}(\rho\varepsilon) + \frac{\partial}{\partial x_i}(\rho\varepsilon u_i) = \frac{\partial}{\partial x_j} \left[\left(\mu + \frac{\mu_t}{\sigma_\varepsilon} \right) \frac{\partial \varepsilon}{\partial x_j} \right] + G_k C_{1\varepsilon} \left(\frac{\varepsilon}{k} \right) - C_{2\varepsilon} \rho \frac{\varepsilon^2}{k} \quad (2.14)$$

where G_k denotes the generation of turbulent kinetic energy due to mean velocity gradients and is defined as

$$G_k = -\overline{\rho u'_i u'_j} \frac{\partial u_j}{\partial x_i} \quad (2.15)$$

In equation (2.15) $-\overline{\rho u'_i u'_j}$ denotes the Reynolds stress which is related to the mean velocity gradient by the Boussinesq hypothesis method and can be shown as

$$-\overline{\rho u'_i u'_j} = \mu_t \left(\frac{\partial u_i}{\partial x_j} + \frac{\partial u_j}{\partial x_i} \right) - \frac{2}{3} \left(\rho k + \mu_t \frac{\partial u_i}{\partial x_i} \right) \quad (2.16)$$

In equation (2.13) Y_M denotes the contribution of the fluctuating dilatation in compressible turbulence to the overall dissipation rate. Basically turbulence could be affected by compressibility through dilatation dissipation. This effect is taken into account via incorporating Y_M into transport equation for kinetic energy k . The term Y_M can be defined as

$$Y_m = 2\rho\varepsilon M_t^2 \quad (2.17)$$

The term M_t is Mach number and μ_t is turbulent viscosity which is computed from combining k and ε and is defined as

$$\mu_t = \rho C_\mu \frac{k^2}{\varepsilon} \quad (2.18)$$

According to equation (2.17), when the flow is incompressible the term Y_M is neglected. The model constants are $C_{1\varepsilon} = 1.44$, $C_{2\varepsilon} = 1.92$ & $C_\mu = 0.09$; and the turbulent Prandtl numbers for k and ε are respectively $\sigma_k = 1$ and $\sigma_\varepsilon = 1.3$.

2.5 Continuity and Momentum Equations

In this section the general form of conservation of mass and momentum equations for gas flow are presented.

2.5.1 Continuity Equation

Continuity equation or the equation for mass conservation is

$$\nabla \cdot (\rho \vec{u}) = S_m \quad (2.19)$$

where S_m is a mass source that is added to the gas phase from the dispersed particle phase; Since our model is two dimensional, equation (2.19) can be written as

$$\frac{\partial}{\partial x} (\rho u_i) + \frac{\partial}{\partial y} (\rho u_j) = S_m \quad (2.20)$$

where u_i and u_j are axial and radial gas velocities respectively.

2.5.2 Momentum Conservation Equations

The axial momentum equation is written as:

$$\frac{\partial}{\partial t}(\rho u_i) + \frac{1}{y} \frac{\partial}{\partial x}(y \rho u_i^2) + \frac{1}{y} \frac{\partial}{\partial y}(y \rho u_i u_j) = -\frac{\partial p}{\partial x} + \frac{1}{y} \frac{\partial}{\partial x} \left[y \mu \left(2 \frac{\partial u_i}{\partial x} - \frac{2}{3} \left(\frac{\partial u_i}{\partial x} + \frac{\partial u_j}{\partial y} + \frac{u_j}{y} \right) \right) \right] + \frac{1}{y} \frac{\partial}{\partial y} \left[y \mu \left(\frac{\partial u_i}{\partial y} + \frac{\partial u_j}{\partial x} \right) \right] + F_x \quad (2.21)$$

where p is static pressure and F_x denotes external body forces in axial direction.

The radial momentum equation is written as

$$\frac{\partial}{\partial t}(\rho u_j) + \frac{1}{y} \frac{\partial}{\partial y}(y \rho u_j^2) + \frac{1}{y} \frac{\partial}{\partial x}(y \rho u_i u_j) = -\frac{\partial p}{\partial y} + \frac{1}{y} \frac{\partial}{\partial y} \left[y \mu \left(2 \frac{\partial u_j}{\partial y} - \frac{2}{3} \left(\frac{\partial u_i}{\partial x} + \frac{\partial u_j}{\partial y} + \frac{u_j}{y} \right) \right) \right] + \frac{1}{y} \frac{\partial}{\partial x} \left[y \mu \left(\frac{\partial u_i}{\partial y} + \frac{\partial u_j}{\partial x} \right) \right] - 2 \mu \frac{u_j}{y^2} + \frac{2}{3} \mu \left(\frac{\partial u_i}{\partial x} + \frac{\partial u_j}{\partial y} + \frac{u_j}{y} \right) + F_y \quad (2.22)$$

where F_y denotes gravitational body force in radial direction.

CHAPTER 3

Turbulent Gas Flow in a Horizontal Pipeline

3.1 Introduction

Pipe flows are generally driven by pressure. As the flow passes through the pipeline, its pressure is decreased due to viscous friction along the pipe walls. Considering the flow in circular pipeline, when fluid enters the pipe and contacts the wall surface, viscous effects cause the boundary layer to develop along the pipeline. As flow further develops downstream the pipe, boundary layer thickness increases at the expense of the shrinking inviscid (zero viscosity) flow region until the boundary layer merges at the centerline of the flow. As of that point, the velocity profile no longer changes with the increase of pipe length, hence the flow is now said to be fully developed. This concept is illustrated by Figure 3.1. In this study the length of pipeline is considered long enough so that flow becomes fully developed somewhere along the pipeline. Also, since the flow from the inlet to the outlet is solved steadily, the behavior of the gas can be studied at every pipe segment regardless of time. In the following sub sections the results of modeling single phase gas flow in pipeline, obtained by CFD software, are studied. The boundary conditions for the case study are set based on the input data provided by ARAMCO as well as literature on black powder movement in a pipeline, discussed in chapter 1. Table 3.1 presents the sales gas properties considered in this study. The range of volume flow rates in standard conditions is minimum 254 mmscfd (million standard cubic feet per day) and maximum 1180 mmscfd. However, the value considered in this chapter is 684mmscfd. Since operating conditions are different from standard conditions, the operating volume flow rate needs to be

computed based on given operating pressure and temperature according to thermodynamics basic principal of gas law [26]:

$$\left[\text{Volume flow rate @operating condition} \right] = \frac{[\text{Volume flow rate @standard condition}]}{[(P_{\text{operating}} / P_{\text{standard}})(T_{\text{standard}} / T_{\text{operating}})]} \quad (3.1)$$

Therefore, 684mmscfd at standard conditions of 14.7psi and 288 Kelvin corresponds to 12mmcf at operating conditions of 900psi and 316 Kelvin. Table 3.2 presents boundary conditions of gas flow at the operating conditions and Table 3.3 shows characteristics of the pipe. It should be mentioned that the pressure shown in Table 3.2 is selected according to data provided by ARAMCO. It is also in accordance with required pressure values in gas pipeline to move black powder particles discussed in literature (See Figure 1.5). For the above volume flow rate, it is clear that the flow is completely turbulent since Reynolds number is considerably greater than Reynolds number criterion which is 2300. In this chapter it is assumed that the density of gas remains unchanged under the effect of pressure & temperature.

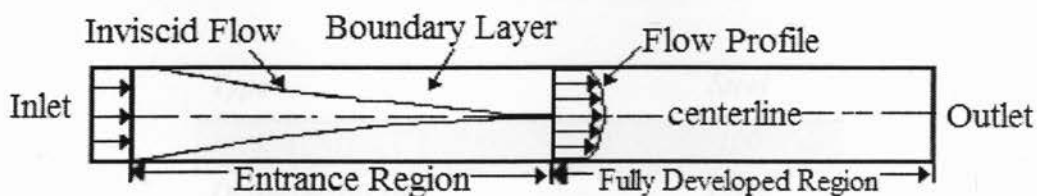


Figure 3.1 Schematic of turbulent flow development in pipe

Table 3.1 Properties of sales gas at 288 °Kelvin

<i>Average Density (Kg/m³)</i>	<i>0.8</i>
<i>Methane (CH₄) Content %</i>	<i>75</i>
<i>Specific heat (C_p) Joule/Kg- Kelvin</i>	<i>2345</i>
<i>Thermal Conductivity W/m-Kelvin</i>	<i>0.0242</i>
<i>Viscosity Kg/m-s</i>	<i>0.000013</i>

Table 3.2 Gas flow characteristics at the inlet at operating conditions

<i>Volume Flow Rate (mmscfd)</i>	<i>684</i>
<i>Volume Flow Rate (mmcf/d)</i>	<i>12</i>
<i>Velocity (v) (m/s)</i>	<i>5</i>
<i>Reynolds number</i>	<i>312615</i>
<i>Pressure (psi)</i>	<i>900</i>
<i>Temperature (Kelvin)</i>	<i>316</i>

Table 3.3 Characteristics of the pipe

<i>Type</i>	<i>Steel</i>
<i>Length (m)</i>	<i>100</i>
<i>Diameters(d) (m)</i>	<i>1.016</i>
<i>Roughness (μm)</i>	<i>30</i>
<i>Cross section Area (m²)</i>	<i>0.81</i>

Table 3.4 Boundary conditions

<i>Model</i>	<i>2D-Axisymmetric</i>
<i>Solver</i>	<i>Pressure based, Steady state, Superficial Velocity</i>
<i>Inlet</i>	<i>Velocity inlet</i>
<i>Outlet</i>	<i>Pressure Outlet</i>
<i>Viscous Model</i>	<i>Standard-k-ε (2eq)</i>
<i>Turbulent Specification Method</i>	<i>Intensity and Hydraulic Diameter</i>

Compared to laminar flows, turbulent flows are more difficult to analyze because additional equations must be solved. There is no general turbulent model available for all types of turbulent flows so it is important to apply a model which is the most appropriate for a specific class of flow. Choosing a suitable model depends on many different parameters such as the physics and characteristics of the flow, level of required accuracy of the solution, available computational resources and required time of the solution. In this study, the model that is used was chosen to be “standard $k-\epsilon$ model” since it is one of the most common turbulence models which gives reasonable accuracy for a wide range of turbulent flows. Table 3.4 presents the boundary condition setup for the model for this case study. In modeling the turbulence, it is assumed that density and viscosity of the gas remain constant. Since the purpose of this chapter is a preliminary preparation for further study on the subject of particle gas flow, focus is placed on analyzing velocity and the turbulent intensity of gas along the pipeline.

3.2 Mesh Consideration and Validation of the Model near the Pipe Wall

Successful computations of turbulent flow require specific consideration when generating the mesh. In cases where a high level of accuracy is required, care should be taken to ensure that turbulence quantities are properly resolved. One of the usual techniques used in mesh sensitivity assessment is the technique of 'doubling'. When using the doubling technique, in order to obtain appropriate mesh resolution, the number of the nodes in the first mesh would double up in the second mesh to examine how the results change or how criteria is satisfied for the next simulation. This method continues until no change (considering the tolerance of $\sim 1\%$) is seen and/or the criteria is addressed, so, moving back to previous mesh. The method used in this study consists of two major steps. The first step is utilizing the model with arbitrary coarse mesh. Subsequently, to confirm the mesh resolution suitability, the law of the wall [26] and the wall friction factor plots (only for the case study which single gas flow is considered) as well as the flow velocity profile are being analyzed. If the results agreed with the criteria requirements then it would be assumed that the mesh sensitivity is suitable otherwise we should proceed to the second step. The second step is to improve the mesh resolution based on the predefined criteria. The mesh resolution, considered for particle-gas flow case studies is 15 (in radial direction) by 2500 (in axial direction). It was found that increasing the mesh sensitivity from 15 x 2500 to 30 x 5000 will not affect the gas velocity profile. Hence the mesh resolution for the model, adopted in chapter 4 was 15 by 2500.

3.2.1 The Law of Wall

Since turbulent flows are significantly affected by the walls, it is critical to do special treatment in defining the grid near the wall where the mean flow changes rapidly and there are shear layers

with a large mean rate of strain. There are three regions in turbulent flow near the wall: 1: viscous wall layer, also known as the viscous sub layer ($y^+ < 5$), where viscous shear dominates, 2: outer turbulent layer where turbulent shear dominates ($y^+ > 30$) and 3: overlap layer, also known as buffer zone ($y^+ = 5$ to 30), where both turbulent and viscous shear play important role. The schematic of these three regions are illustrated in Figure 3.2. The law of the wall follows the linear viscous relation from the wall to about $y^+ = 5$ which is written as

$$y^+ = u/u^* \quad (3.2)$$

In the above relation the term u denotes the velocity as function of the density, the viscosity, the wall shear stress and the thickness at the edge of the outer layer. On the other hand, u^* is a quantity which is termed “the friction velocity” since it has dimensions of LT^{-1} although it is not really a flow velocity. After, the flow profile curves over to merge with the logarithmic law at about $y^+ = 30$ which is the outer turbulent layer. According to the law of the wall, adjacent cells at the wall region should be prevented from being placed in the overlap layer. Therefore, to satisfy the law of the wall the plot of y^+ at the wall region should fall within the range of 1 to 5 or greater than 30. In the current case study which only the flow of gas is considered, the mesh resolution is improved in such a way that y^+ would fall within the range of 1 to 5. The preliminary mesh for the type of pipe geometry with characteristics presented by Table 3.3 has 25551 nodes. In the case where only natural gas flow is considered, the volume flow rate of 684mmscfd (12mmcfd) and density of 0.8 Kg/m^3 is considered. After mesh improvement, the number of nodes increased from 25551 to 87556 nodes. Figure 3.3 illustrates the y^+ plot. It can be seen that y^+ is about 1.4 along the pipe at the wall which indicates that the mesh resolution considered in this study is acceptable near the wall region for single gas flow.

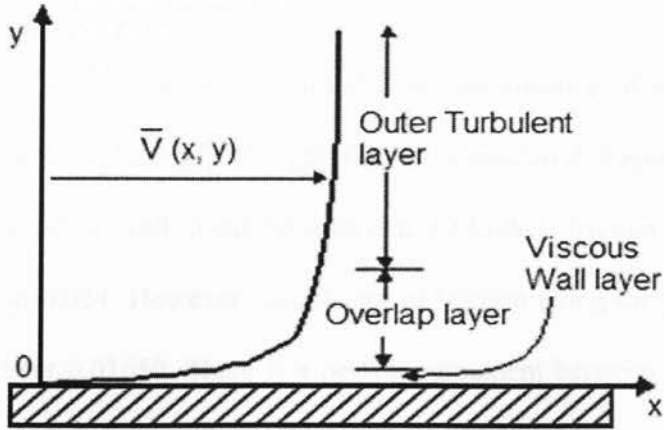


Figure 3.2 Velocity profile distribution in turbulent flow near the wall [27]

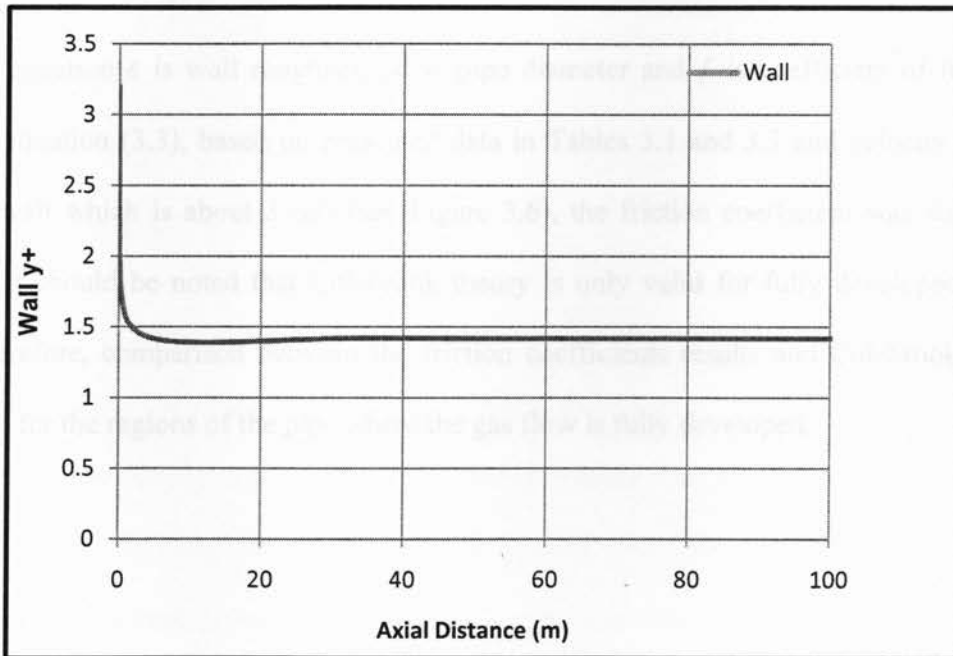


Figure 3.3 y^+ Plot at the wall

3.2.2 Evaluation of Friction Coefficient

The results obtained for the wall friction would also be an indication of mesh suitability of the model for the case study where only the gas flow is considered. Figure 3.4 shows friction coefficients along the pipeline wall. It can be seen that the highest friction coefficient appears at the inlet which is about 0.024. However, coefficient of friction along the pipe wall in the fully developed region is about 0.01650. There is a perfect agreement between the results of friction factor coefficient in this study case and the theory. The theoretical relation applied as criterion is Colebrook interpolation formula [28] which is written as

$$\frac{1}{f^{1/2}} = -2 \log \left[\frac{2.51}{Re f^{1/2}} + \frac{\epsilon/d}{3.72} \right] \quad (3.3)$$

In above equation ϵ is wall roughness, d is pipe diameter and f is coefficient of friction. By applying equation (3.3), based on presented data in Tables 3.1 and 3.3 and velocity of the gas near the wall which is about 3 m/s (see Figure 3.6), the friction coefficient was computed as 0.01606. It should be noted that Colebrook theory is only valid for fully developed turbulent flow. Therefore, comparison between the friction coefficients results and Colebrook theory is applicable for the regions of the pipe where the gas flow is fully developed.

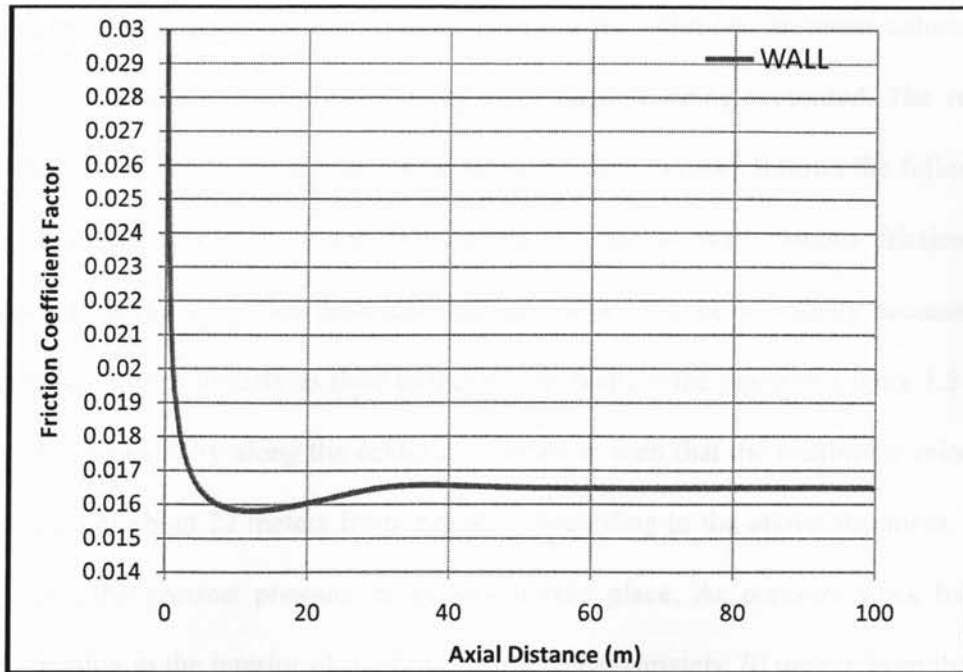


Figure 3.4 Variation of the skin friction coefficient along the axial length of the pipe

3.3 Gas Flow Velocity

As flow appears in a fully developed pattern, the inviscid core disappears and the flow becomes entirely viscous. As the flow progresses downstream the viscous boundary layer grows and the axial flow near the wall becomes retarded by viscous friction. That results in an injection of fluid (gas) into the region away from the wall to satisfy the mass conservation [29]. According to White [30], in turbulent flows, because of the fluctuations, every velocity and pressure term in continuity and momentum equations is a rapidly varying random function of time and space. Since these instantaneous fluctuations variables cannot be solved by mathematical techniques no single pair of random functions of velocity and pressure is known to be a solution to the continuity and momentum equations. Therefore, the best way dealing with that is averaging these

fluctuations over some period domain and presenting the solutions as mean values over that domain. This is generally the way results in this study are being presented. The relationship between velocity and pressure fluctuations in turbulent flow in pipes follows the following basic principal: When the pressure of the flow decreases due to wall viscous friction, velocity increases accordingly. When flow becomes fully developed, its mean velocity becomes constant and flow pressure drops linearly as fluid moves downstream in the pipeline. Figure 3.5 shows the variations of axial velocity along the centerline. It can be seen that the maximum velocity of the gas flow occurs at about 22 meters from the inlet. According to the above argument, that is the point in which the greatest pressure drops would take place. As pressure work balanced by viscous dissipation in the interior of the flow, within approximately 70 meters from the inlet, the flow eventually becomes fully developed and continues with constant mean velocity of ~ 5.9 m/s. The integral of the dissipation functions over the flow field is equal to work done by pressure forces to drive the fluid through the pipe. The viscous dissipation rate is a quadratic function of spatial derivatives of components of fluid velocity which gives the rate at which mechanical work (e.g. pressure) is converted into heat in a viscous fluid per unit volume. It should be noted that no work can be done by the wall shear stresses because velocity at the wall is zero.

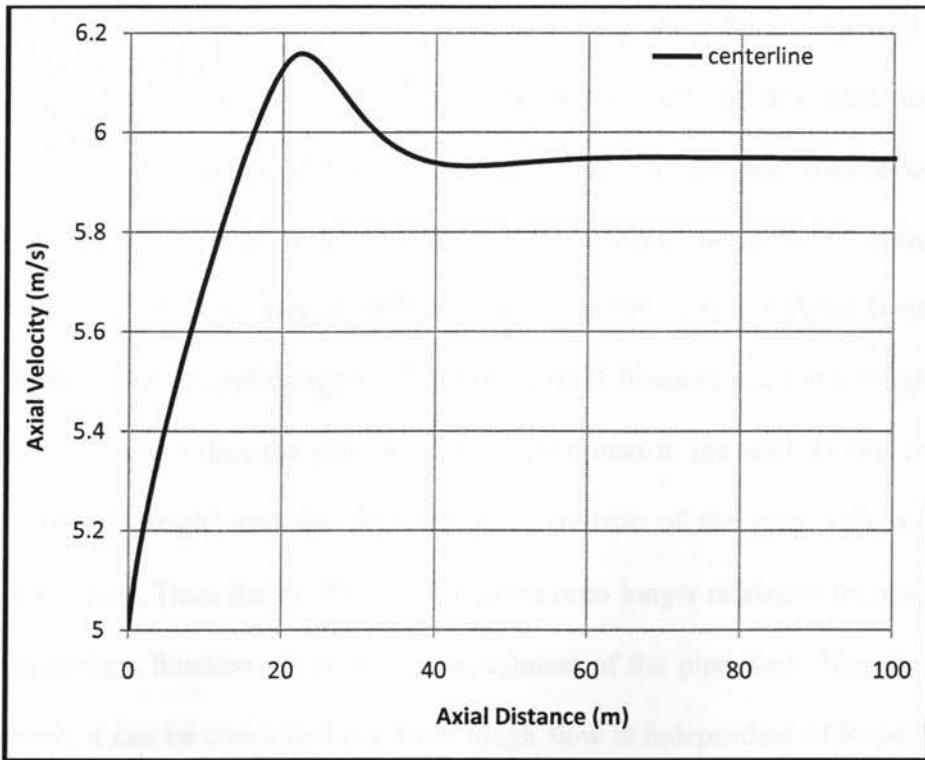


Figure 3.5 Axial velocities along the centerline vs. axial distance

Basically, pressure drop in turbulent flow is strongly affected by wall roughness. Nikurads [31] simulated and recorded roughness of the inner wall of the pipe experimentally and measured the pressure drops and flow rates and correlated friction factor versus Reynolds number. Nikurads correlation shows that turbulent friction increases monotonically with the increase of roughness ratio which is the ratio of pipe wall roughness and pipe diameter. Therefore, in cases with larger relative wall roughness, the effect of viscous friction is greater than cases with smaller roughness. The smoothness of the flow is also dependent on the roughness. According to the studies of Smith [32], turbulent flow of fluids in circular pipes falls into two categories depending upon the relationship between the viscous wall layer of the fluid and the roughness of

the pipe wall. The first category of turbulent flow of fluids is when the viscous wall layer of the fluid next to the pipe wall covers the roughness of the pipe. In this case, the dominant characteristic of the pipe wall is the viscosity of the fluid, and the skin friction coefficient is directly related to the viscosity. In this condition flow is said to be "smooth" even though the flow is classified as turbulent. Hence, skin friction in smooth turbulent flows is dependent on Reynolds number. The second category of turbulent fluid flows is when the roughness of the pipe wall becomes larger than the sub layer of the fluid next to the wall. In this condition the flow is said to be "rough" and the dominant characteristic of the pipe wall is the relative roughness of the wall. Thus, the coefficient of friction is no longer related to the viscosity of the fluid but is directly a function of the relative roughness of the pipe wall. Therefore, based on above argument, it can be concluded that fully rough flow is independent of Reynolds number. Figure 3.6 presents velocity variations in the radial direction at four different segments along the pipeline. The horizontal axis intersecting the vertical axis indicates centerline. By looking at Figure 3.6, it can be seen that the velocity profile has greatest slope around 25 meters from the inlet. That is the point where the highest velocity is achieved by the gas. Thereafter, as flow proceeds downstream, the slope lowers until about 70 meters axial distance from the inlet. From this point to the end of the pipeline the velocity profile of the gas flow stays unchanged. The graphs shown by Figure 3.6 are very informative in studying and interpreting the results over the cross section area of the pipe, especially when behavior of particles is to be studied along with gas flow.

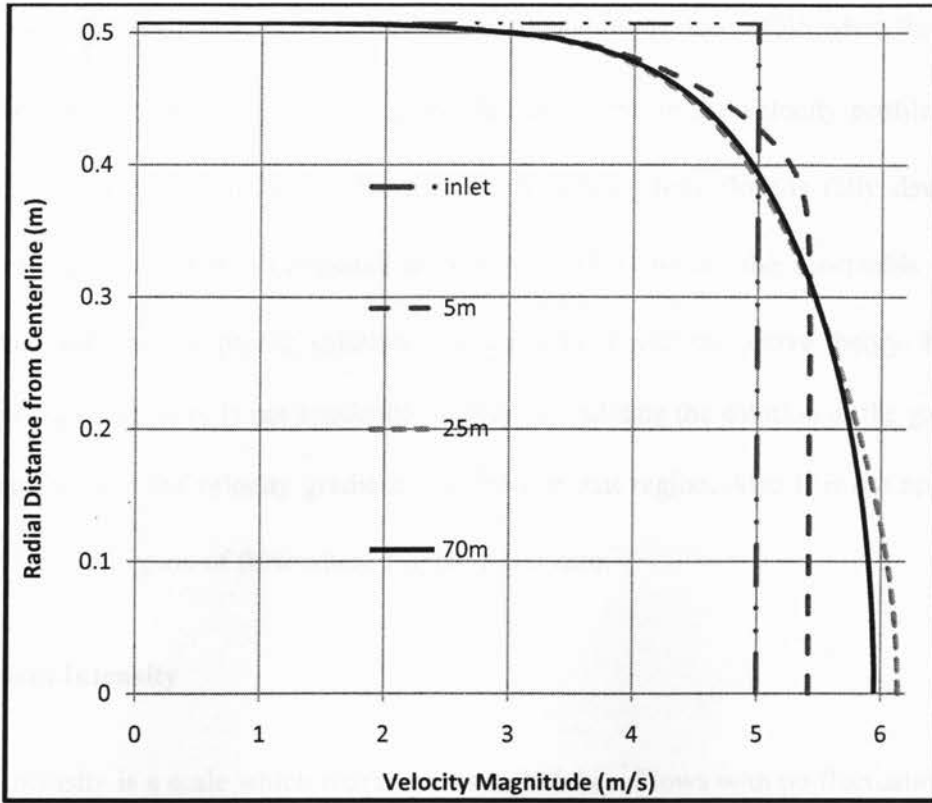


Figure 3.6 Radial variations of velocity vs. various pipeline stations

3.3.1 Validation of Gas Flow Velocity Profile

In this study the validation of the solution for the turbulent velocity profile is evaluated using an empirical correlation, the so called “power-law velocity profile” [33] which is written as

$$\frac{\bar{u}}{u_c} = \left(1 - \frac{r}{R}\right)^{\frac{1}{n}} \quad (3.5)$$

where \bar{u} is denoted as the mean velocity at any point on the velocity profile, u_c is velocity at the core of the flow, R is pipe radius and r is radial distance correspondent to the mean velocity. The value of n is denoted as function of Reynolds number. According to “power-law velocity

profile” the solution of the velocity profile in turbulent flow is acceptable when the value of n falls between $n=6$ and $n=10$. Considering an arbitrary point on the velocity profile, 70 meters from inlet, in Figure 3.6 with $r = 0.3\text{m}$ and $\bar{u} = 5.42\text{m/s}$ where flow is fully developed and $u_c \sim 5.95\text{m/s}$ the value of n is computed to be 9.6 which is within the acceptable range. This indicates that our velocity profile solution is in agreement with the above theory. It should be noted that the above theory is not applicable in order to validate the solution of the gas flow near the wall region since the velocity gradient is infinite at that region. Also it is not appropriate to apply near the core region of flow where r approaches zero.

3.4 Turbulent Intensity

Turbulent intensity is a scale which characterizes turbulence. Flows with no fluctuations in speed or direction would have a turbulent Intensity of zero. However, this is an idealized case that would never occur. Figure 3.8 is illustrating the intensity percentage of turbulent flow throughout the centerline of the pipe. The range of turbulent intensity, as it is shown, varies approximately from 1.4% to 3.4% at centerline and from 1.4 to 5.5% at all stations of the pipeline. In general, this is quite realistic for the fluid flow in not-so-complex devices like large pipes as considered in this study. As shown by Figure 3.8, the turbulent intensity is not varying after the flow enters the fully developed region. By comparing the results of gas flow velocity and the results of gas flow turbulent intensity it can be seen that the greatest fluctuations of turbulent intensities fall within the sections of the pipe where flow is not yet fully developed. This is the region where the inviscid and boundary layers exist along the fluid flow. Generally, velocity and pressure fluctuations are greater in the entrance region of flow in comparison with the fully developed region. Since these fluctuations greatly affect turbulent intensity stability, it is expected to see

variation of turbulent intensities over entrance the region of fluid flow. According to Johansson et al. [34], turbulent intensity is directly proportional to the Root-Mean-Square (RMS) or Standard Deviation of the turbulent velocity fluctuations at a particular location over a specified period of time. Root-Mean-Square (RMS) or Standard Deviation is the square root of variance. The concept of variance, in this study, is the statistical measurement of the dispersion of velocity fluctuation data about a mean value of velocities over the time domain. Figure 3.7 shows picture of velocity fluctuations vs. time and RMS of these fluctuations.

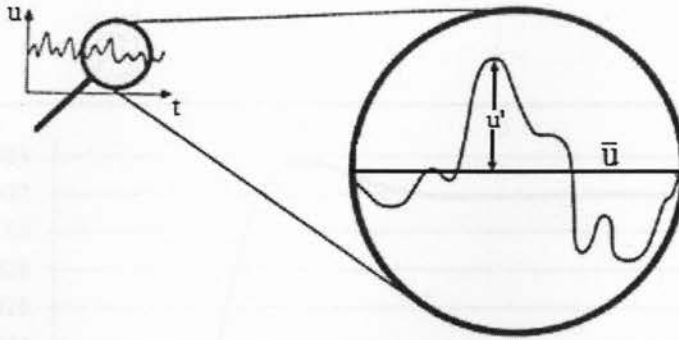


Figure 3.7 Illustration of RMS (u') & velocity fluctuation data about a mean value of velocity

General definition of turbulent intensity can be expressed as

$$T.I. = \frac{u'}{\bar{u}} \quad (3.6)$$

where u' is Root-Mean-Square (RMS) or Standard Deviation of the turbulent velocity fluctuations at a particular location over a specified period of time and \bar{u} is the mean velocity.

When the flow is fully developed the turbulent intensity can be expressed as a function of Reynolds number at the core region:

$$T.I. = 0.16 R_e^{-1/8} \quad (3.7)$$

According to this relation, the turbulent intensity is inversely proportional to the flow's Reynolds number; on the other hand, the Reynolds number is directly proportional to the velocity. So, turbulent intensity is inversely proportional to average velocity of gas flow. In our case, considering that the velocity in the fully developed region at the centerline is about 5.9 m/s, the corresponding Reynolds number can be computed as 399,627. So, based on above definition turbulent intensity would be computed as 3.2% which is precisely in agreement with our predicted results shown by Figure 3.8.

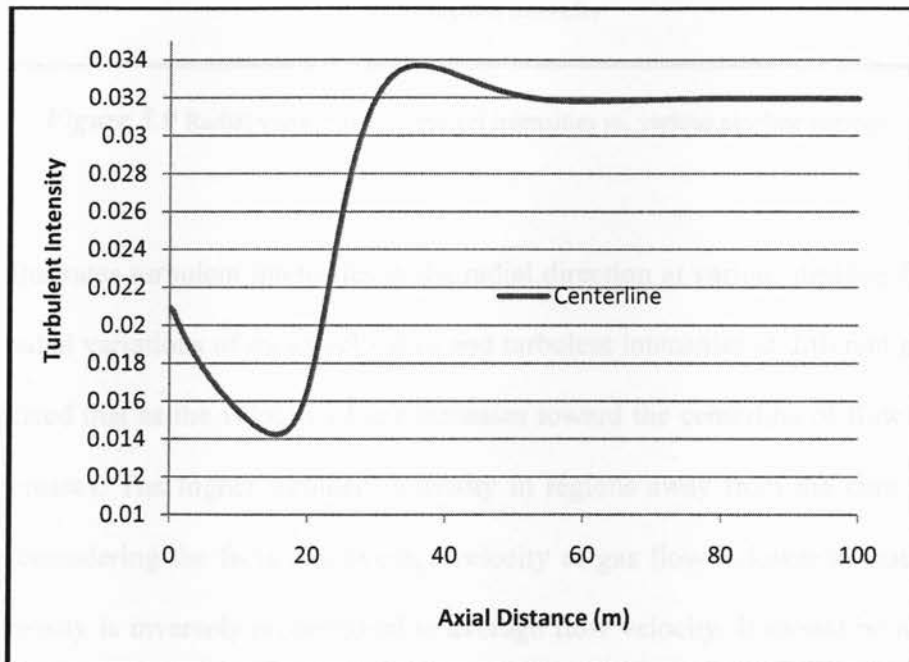


Figure 3.8 Turbulent intensity vs. axial distance

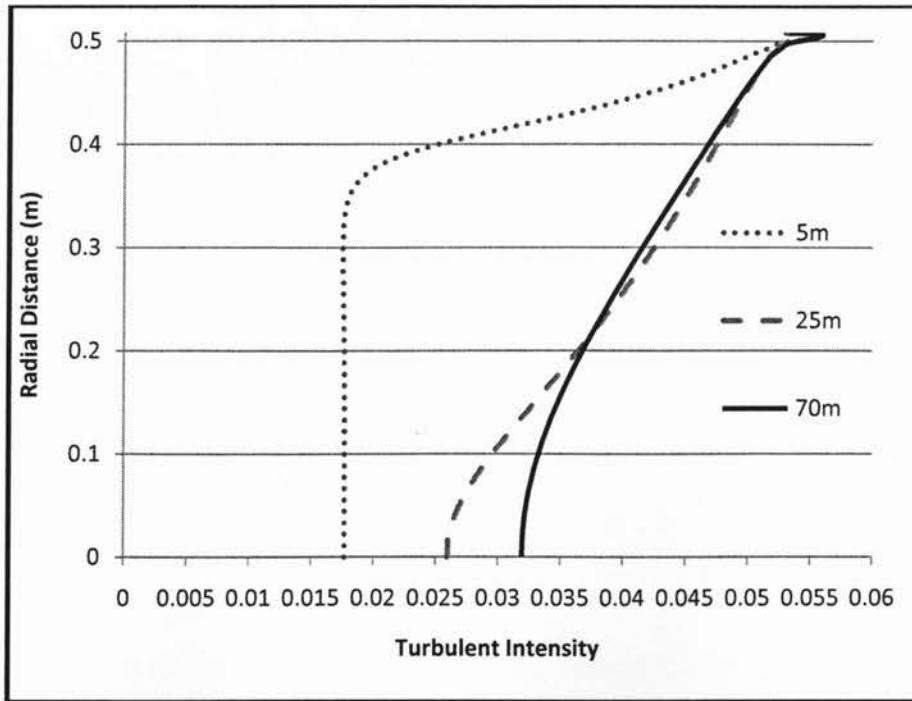


Figure 3.9 Radial variations of turbulent intensities vs. various pipeline stations

Figure 3.9 illustrates turbulent intensities in the radial direction at various pipeline locations. By comparing radial variations of mean velocities and turbulent intensities at different pipe stations, it can be noticed that as the velocity of gas increases toward the centerline of flow its turbulent intensity decreases. The higher turbulent intensity in regions away from the core flow can be justified by considering the facts that average velocity of gas flow is lower in that region, and turbulent intensity is inversely proportional to average flow velocity. It should be noted that all the radial variations of turbulent intensities illustrated in this study are indeed displaying turbulent intensities within the outer turbulent layer where turbulent shear predominates. The outer turbulent layer, in this case study, begins approximately 0.8 cm from the wall. Of course in the region between the wall inner surface and outer turbulent layer, flow velocity is approaches zero; hence there is no turbulent intensity.

CHAPTER 4

Particle Laden Flow Modeling in Horizontal Gas Pipeline

4.1 Introduction

In recent years considerable advances have been made on the modeling of solid gas flows in pipe. There are vast applications in most chemical, petroleum, and pharmaceutical industries which are involved with solid gas flows. For instance, in the chemical industry, almost all chemical processes involve solid handling. In other processes such as pneumatic conveying, coal combustion, and fluid catalytic cracking, turbulent gas particle flows are encountered. Solid gas flows are denoted as one of the categories of multiphase flows. Generally, in multiphase flow, a phase can be defined as a class of material that has a specific inertial response to the potential field in which it is immersed. For instance, different sized solid particles of the same kind of material can be treated as different phases since each collection of particles with the same size will have a similar dynamic response to the flow. Basically solid gas flows are categorized into three flow regimes; the first regime is particle laden flow, the second is pneumatic transport and the third, fluidized bed. In this study the flow regime is considered as a particle laden flow which is flow of the discrete particles in a continuous gas. Particle laden flow is the case when dispersed second phase occupies a low volume fraction, even though the mass loading of the dispersed phase could be greater than the mass of the continuum fluid. The dispersed second phase consists of spherical particles dispersed in the fluid phase. Generally, there are two different approaches that are taken to apply computational fluid dynamics to solid gas flow regimes. The first approach is Eulerian-Eulerian which is based on continuum mechanics and

treats the two phases of the solid and the gas as interpenetrating continua. The second approach, applied in this study, is Lagrangian-Eulerian. In this approach the gas is treated as a continuum fluid, while the solid phase is treated as a dispersed phase and solved by tracking many numbers of particles. It should be reminded that when considering the solid phase as a dispersed phase, it is assumed that particles are dilute enough so that particle-particle interactions and the effects of the particle volume fraction on the gas phase are negligible. In the present study, the term dilute refers to fairly low volume fractions of particle, often less than 10 to 12 percent, regardless of the mass loading of the discrete phase which may exceed that percentage. In this study, simulation of the results can be generalized as prediction of the turbulent effects on the dispersed particles due to turbulent eddies present in the continuous phase and computation of the particle trajectory using a Lagrangian formulation that includes the discrete phase inertia, the hydrodynamic drag, and the force of gravity. Computation of particle trajectories involves integration over time of the force balance on the particle. Table 4.1 presents the characteristics of the pipeline. The particle tracking simulation is implemented from the inlet to the outlet of the pipe. The flow of gas at the particle injection point is selected to be in the completely developed region so that simulation of particle movements from the injection point all the way down to the pipe's outlet is being conducted in consistently fully developed gas flow where no inviscid flow exists and the boundary layer is perfectly merged at the centerline of flow. Since the density of the particles is relatively large compared to the gas, the effect of gravity is taken into account; therefore, the pipe model is constructed as 2 dimensional and not axis-symmetric to be able to investigate the effect of the gravity force on particles. The predictions of particle laden flow are simulated for various cases. In first case, instantaneous injection, a large concentration of particles with different sizes is injected into the gas flow for duration of one tenth of a second. So, by knowing

the mass flow rate of particles, the total mass of dispersed particles can be determined. In the first case study both continuous and discrete phase simulations are dependent on time. By selecting the unsteady (transient) solving method, controlling the simulation of the solutions can be possible over the desire time domain since particles are not continuously injected. The defined time domain is selected, based on the gas velocity, diameter and length of the pipeline. The determination of quantities of particle concentrations is based on criterion given provided by ARAMCO. According to this criterion, under standard conditions, the particle mass loading is 1.84 grams for every million standard cubic feet of sales gas. In other case studies, the flow of gas is solved using steady state technique and particles are tracked as a function of time. Also, the change of the natural gas density as a result of temperature and pressure changes is taken into account. By carefully comparing the results from the case studies for certain particle sizes, it can be noticed that the drag force of the natural gas flow increases when its density increases. The simulation of particle behavior in turbulent gas flow are only providing general prediction of how particles respond in the effect of the gas flow since turbulent gas flow regimes are basically characterized by chaotic and stochastic property changes. Therefore, for all case studies, dispersion of particles in turbulent gas flows is modeled using a stochastic tracking approach. Using this approach, the prediction of particle dispersion is implemented through the integration of trajectory equations for every particle using the instantaneous gas velocity (equation 2.5) along the particle path. Hence, the effect of the turbulence on the dispersed particles can be predicted by computing the trajectories for certain numbers of particulates. The input file to the CFD model for every case study, discussed in this chapter, is presented in Appendix.

Table 4.1 Characteristics of the pipe

<i>Type</i>	<i>Steel</i>
<i>Length (m)</i>	<i>25</i>
<i>Diameter (m)</i>	<i>1.016</i>
<i>Wall inner surface Roughness (μm)</i>	<i>30</i>

4.2 Validation of the Model Approach

In order to examine the integrity and the validity of the model approach taken in this study, an exact comparison with the numerical work done by Lun [35] was done by solving a specific case. The approach used by Lun is the standard $k-\varepsilon$ model which is the same approach applied in this study but for different model geometry and boundary conditions. C.K.K. Lun studied the impact of particle mass loading on the mean fluid velocity distribution in a vertical pipe with specific diameter for different particle sizes. The case considered by Lun used 0.2mm size particles, with a mass loading of 0.5 Kg particles per cubic meter of air, carried by air flow with a bulk velocity of 10.6 m/s. The mean fluid velocity is normalized by fluid bulk velocity and is shown as term U_x^* . As illustrated by Figure 4.1, various mesh sensitivities were examined in order to obtain an appropriate mesh resolution using the “mesh doubling method”. It turns out that the velocity profile of air will remain unchanged by further increasing the mesh sensitivity of the model with 60 x 2000 mesh resolution. Therefore, 60 x 2000 mesh model is selected as suitable to solve this particle-gas flow. As illustrated in Figure 4.2, excellent agreement can be found between the present simulated results and results obtained by Lun. This agreement validates the model approach applied in this study.

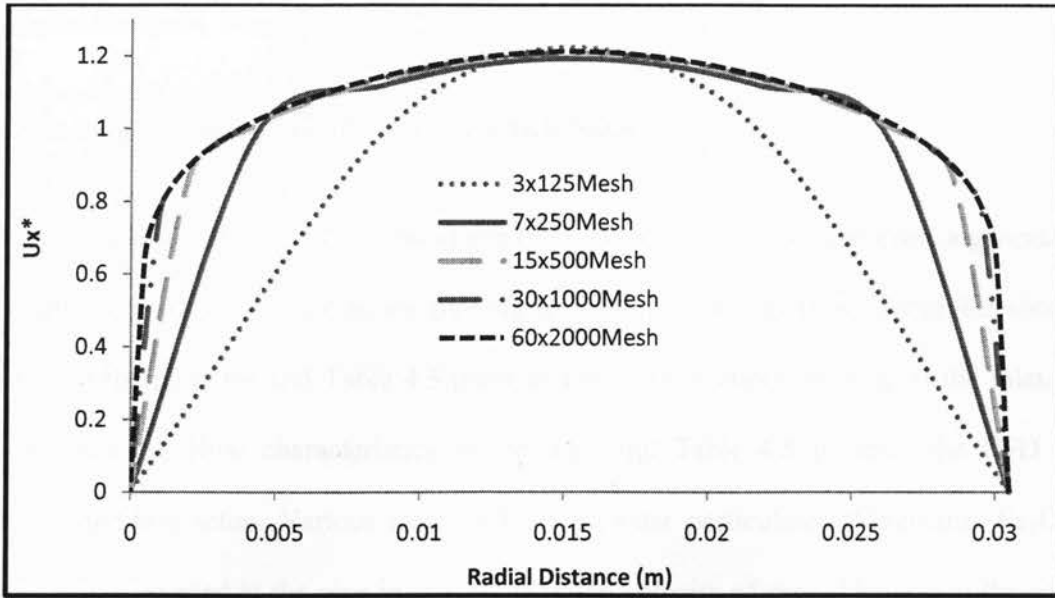


Figure 4.1 Various mesh sensitivities of mean air velocity distribution with zero particle mass loading for bulk air velocity of 10.6m/s

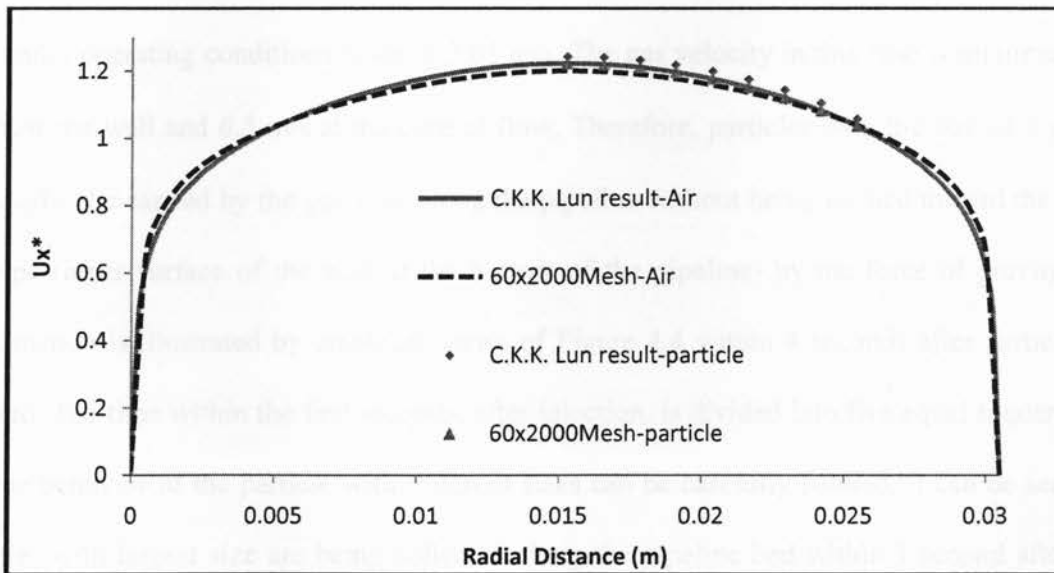


Figure 4.2 Comparison of our results with results obtained by C.K.K Lun [35] for particle mass loading of 0.5.

4.3 Results Analysis

4.3.1 Instantaneous Injection of Diverse Particle Sizes

Graphical simulation of the particles movement is very informative since it gives a general sense of how different sizes of particles are moving in the turbulent gas flow. Table 4.2 shows the properties of the particles and Table 4.3 presents the particle injection setup at the inlet. Table 4.4 shows the gas flow characteristics at the inlet and Table 4.5 presents the CFD model boundary condition setup. Various sizes of black powder particulates (Magnetite, Fe_3O_4) are instantaneously injected at the pipe inlet with an initial velocity of zero. The size of the particles ranges from $1\ \mu\text{m}$ to $100\ \mu\text{m}$. The gas flow is fully developed from the injection point to the pipeline outlet. This is shown by Figure 4.3. The total weight of injected particles is 50 grams which corresponds to 500 grams per seconds for duration of 0.1 second. According to the literature, the minimum gas velocity to drag and move a $1\ \mu\text{m}$ magnetite particle in a 40 inch pipe under operating conditions is about 3.65 m/s. The gas velocity in this case is minimum 3.75 m/s near the wall and 6.5 m/s at the core of flow. Therefore, particles with the size of $1\ \mu\text{m}$ are expected to be carried by the gas flow along the pipeline without being pushed toward the bed of the pipe (inner surface of the wall at the bottom of the pipeline) by the force of gravity. This phenomenon is illustrated by graphical views of Figure 4.4 within 4 seconds after particles are injected. The time within the first seconds, after injection, is divided into five equal sequences so that the behavior of the particle with different sizes can be carefully studied. It can be seen that particles with largest size are being collected along the pipeline bed within 1 second after they are injected into the continuum flow. This is because the gravity force on large particles dominates the drag force caused by gas flow. By looking plots Figure 4.4 (d), (e) and (f), it can

be observed that even though particles are being placed over the pipeline bed, they are still being moved toward the outlet. However, their velocity is as low as 2.7 m/s as shown by the color scale in Figure 4.5 (b).

Table 4.2 Particle properties

<i>Material</i>	<i>Black Powder-Magnetite-Fe₃O₄</i>
<i>Density (Kg/m³)</i>	<i>5150</i>
<i>Specific gravity</i>	<i>5.15</i>
<i>Min Diameter (m)</i>	<i>10⁻⁶</i>
<i>Max Diameter (m)</i>	<i>10⁻⁴</i>
<i>Mean Diameter (m)</i>	<i>10⁻⁵</i>
<i>Shape</i>	<i>Sphere</i>

Table 4.3 Particle injection setup

<i>Injection Type</i>	<i>Inlet Surface</i>
<i>Injection Angle</i>	<i>Face normal direction</i>
<i>Injection Duration (s)</i>	<i>0.1</i>
<i>Initial Velocity of the particles at the injection point (m/s)</i>	<i>0</i>
<i>Distribution</i>	<i>Logarithmic</i>
<i>Turbulent Dispersion of particles</i>	<i>Stochastic tracking</i>
<i>Tracking Particles</i>	<i>Un-steady</i>
<i>Total Weight of particles injected (gm)</i>	<i>50</i>
<i>Mass Flow Rate of Particles (gm/s)</i>	<i>500</i>

Table 4.4 Characteristics of the gas flow at the inlet at operating conditions

<i>Volume Flow Rate (m³/s)</i>	<i>5.295</i>
<i>Volume Flow Rate (mmcf/d)</i>	<i>16.156</i>
<i>Velocity (m/s)</i>	<i>6.5375</i>
<i>Reynolds number</i>	<i>409,000</i>
<i>Pressure (psi)</i>	<i>900</i>
<i>Temperature (Kelvin)</i>	<i>316</i>
<i>Density (kg/m³)</i>	<i>0.8</i>
<i>Viscosity Kg/m-s (μ)</i>	<i>0.0000133</i>

Figure 4.2 Gas velocity profile at the inlet and outlet of the pipe before pipe expansion

Table 4.5 CFD model boundary condition setup

<i>Model</i>	<i>2D-inlet-wall-outlet</i>
<i>Solver</i>	<i>Pressure based, Un-Steady, Superficial Velocity</i>
<i>Inlet</i>	<i>Velocity inlet-Fully developed flow</i>
<i>Outlet</i>	<i>Pressure Outlet</i>
<i>Viscous Model</i>	<i>Standard-k-ϵ (2eq)</i>
<i>Turbulent Specification Method</i>	<i>Intensity and Hydraulic Diameter</i>

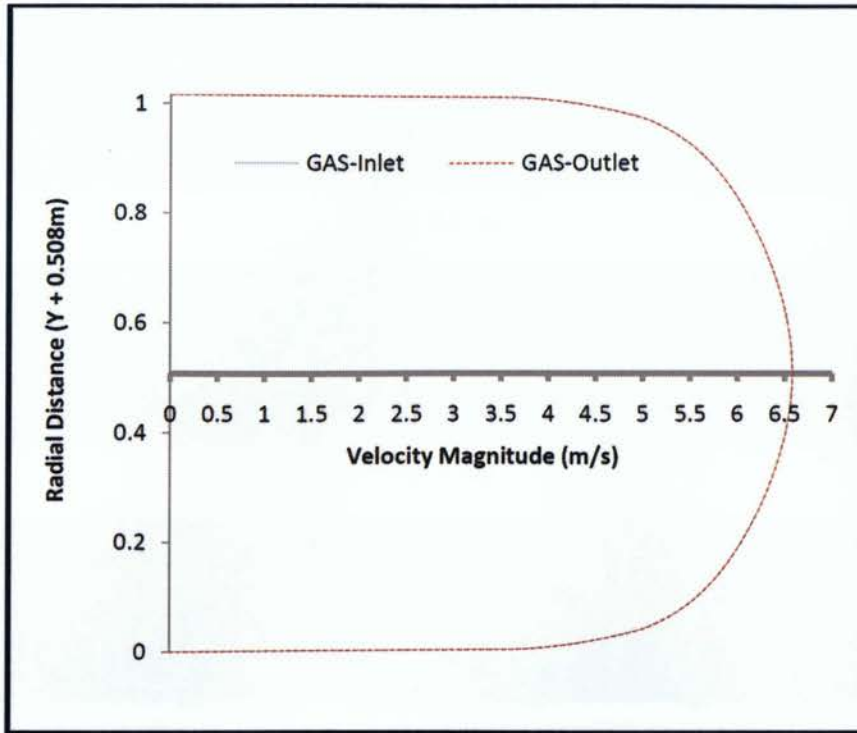
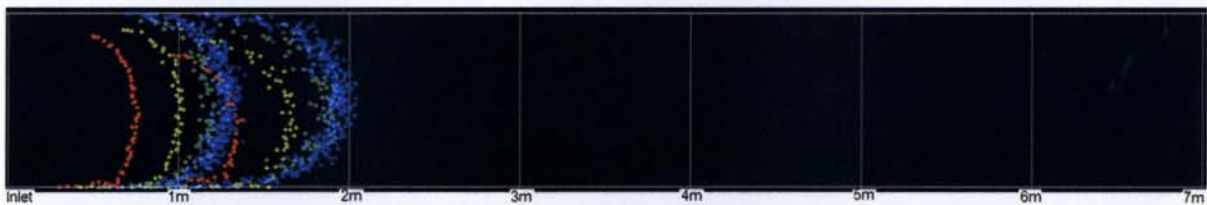
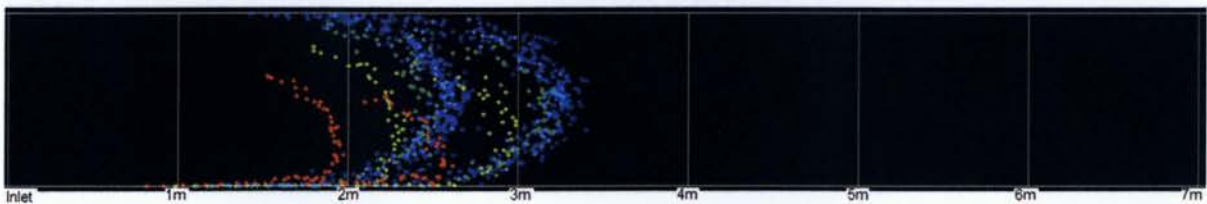


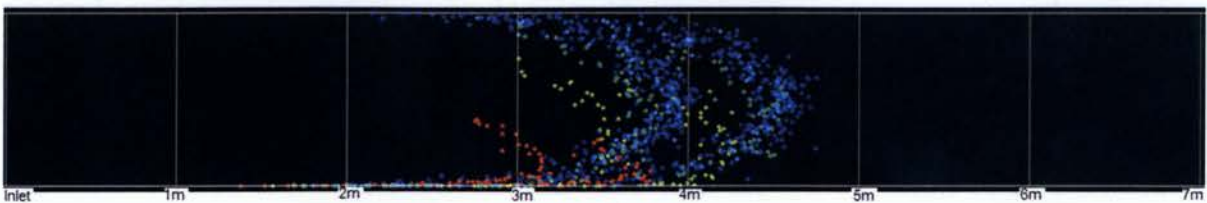
Figure 4.3 Gas velocity profile at the inlet and outlet of the pipe before particle injection



(a) 0.2 sec



(b) 0.4 sec



(c) 0.6 sec

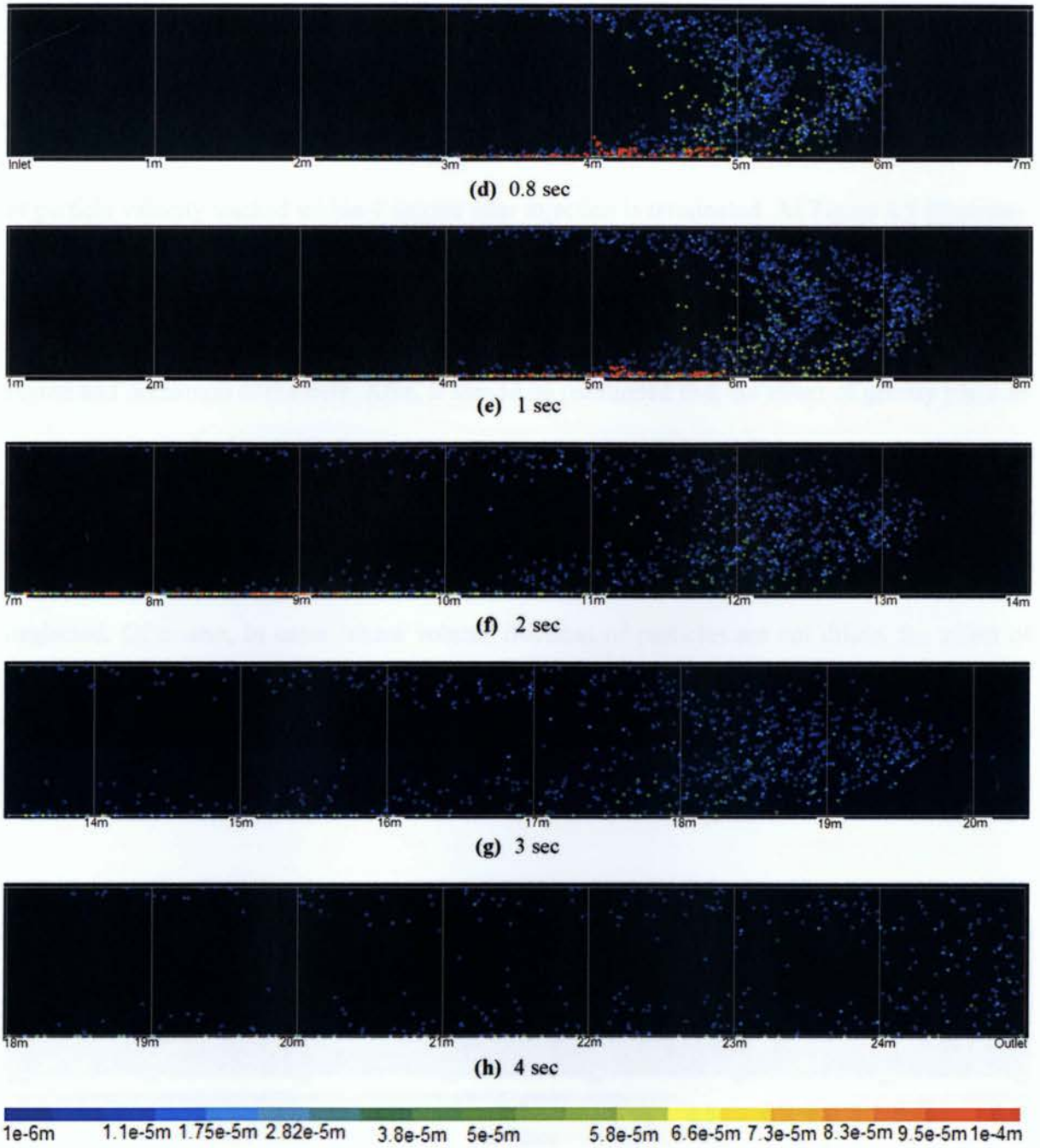
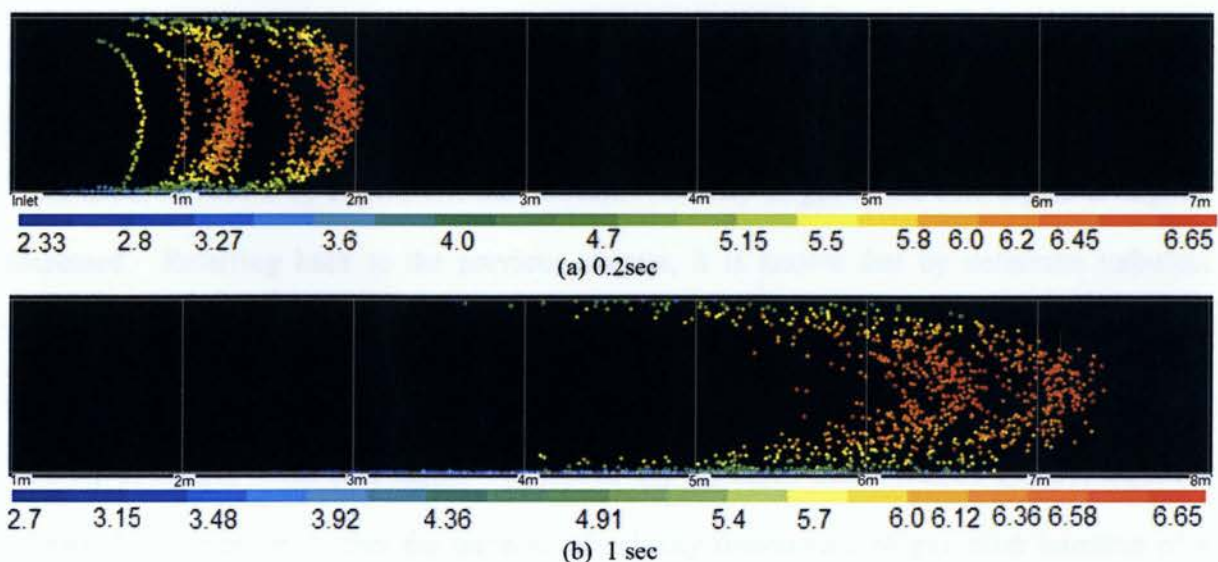


Figure 4.4 Graphical tracking of black powders particulates, carried by fully developed gas flow, from injection point to the outlet within 4 seconds from (a) to (h). Colored by diameter (m)

Not only particles with the largest size but also most of those with smaller sizes (30 to 40 μm) eventually are pushed toward the bottom of the pipeline by gravity force before they reach the

outlet. However, along with $1\ \mu\text{m}$ particles, few particles with sizes as big as about $40\ \mu\text{m}$ are still flowing toward the outlet. Other than size, velocity variations of particles are also dependent on their position immediately after they are injected into gas. Figure 4.5 is a graphical simulation of particle velocity tracked within 4 second after injection is terminated. As Figure 4.5 illustrates, clouds of particles close to the wall region have lower velocities in comparison with particles toward the core of flow. That is because the gas flow velocity is at its minimum near the wall region and maximum at the core. Also, it should be mentioned that the effect of gravity plays an important role in increasing the particles velocity toward the lower wall by accelerating particles in the y direction. In this study, as mentioned earlier, it is assumed that particles are dilute in terms of volume fraction of the gas so that the effect of particle-particle interactions can be neglected. Of course, in cases where volume fractions of particles are not dilute, the effect of collision between particles should be taken into account.



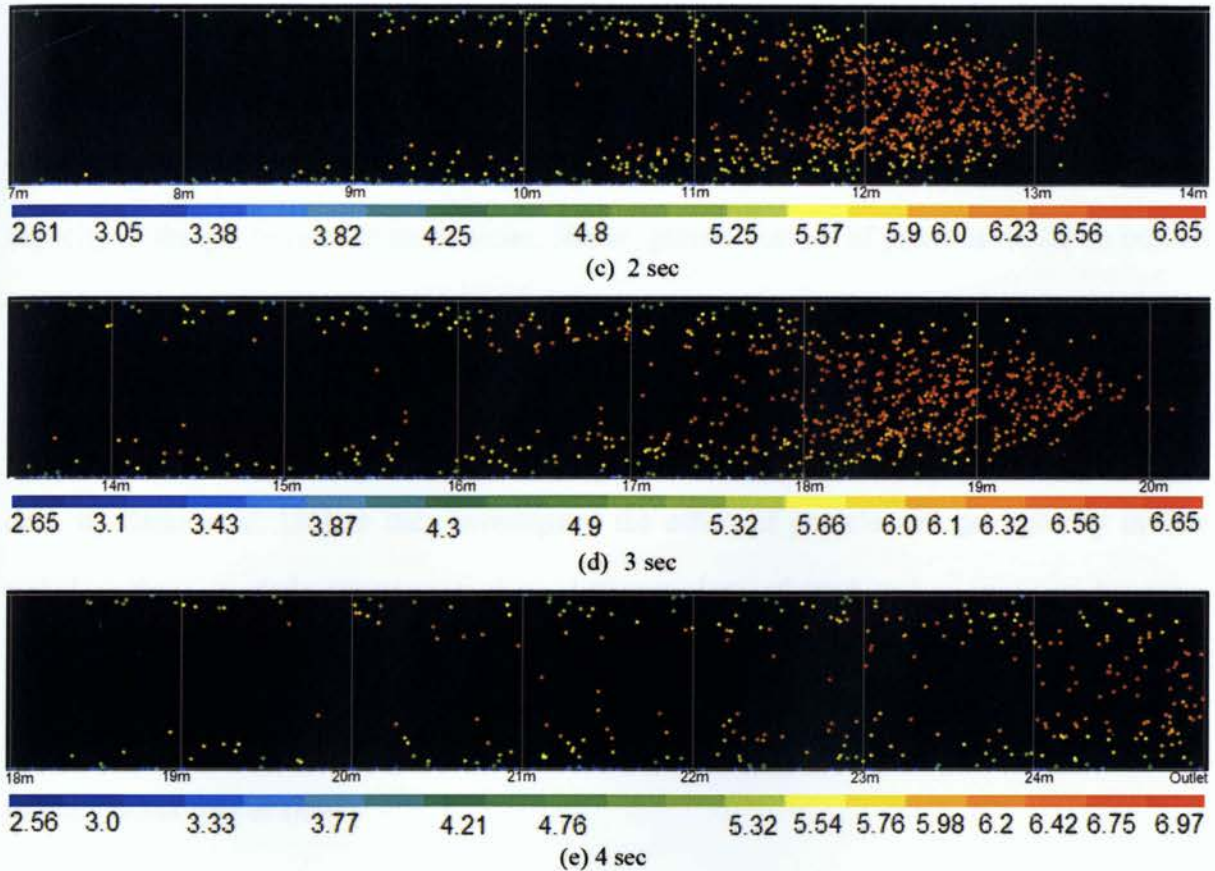


Figure 4.5 Graphical tracking of black powders particulates, carried by fully developed gas flow, from injection point to the outlet within 4 seconds from (a) to (e). Colored by velocity magnitude (m/s)

Figure 4.6 illustrates the velocity profile of gas before and after injection. It can be seen that the mean velocity of gas is slightly decreased at the core region (region along the pipeline where is limited to radial distance from 0.4m to 0.6m) of the flow as a result of particle dispersion; on the other hand, as shown by Figure 4.7, the turbulent intensity of gas in the core region is slightly increased. Referring back to the previous chapter, it is known that by definition turbulent intensity is directly proportional to root mean square of velocity fluctuations and inversely proportional to mean velocity. It is reasonable to assume that velocity fluctuations and mean velocity of the gas in the core region are respectively increased and decreased as a consequence of particles dispersion. In fact the increase of velocity fluctuations of gas, after injection of a

relatively high mass load of particles within a short period, can be expected at the core region of the flow where mean gas velocity is at its maximum. Indeed the higher gas velocity at the core region results in larger drag force of the gas, as carrier flow, and subsequently enhances the capacity of the gas to carry more particles. Hence, greater number of particles would be pushed toward the core after they are injected into flow. Also, sudden injection of a high mass load of particles would act like a barrier against the fluid flow and so results in lowering the mean velocity of gas. The above analysis of results can be precisely validated by experimental work done by Staki et al. [36] as they investigated the effect of particles on gas velocity in free turbulent flow. In their experiment, three different sizes of sand and quartz particles were examined. The sizes of particles they used ranged from 1 to about 800 μm . Their experimental results showed that increase of mass loading of particles induces a decrease in the mean gas velocity in the core of flow.

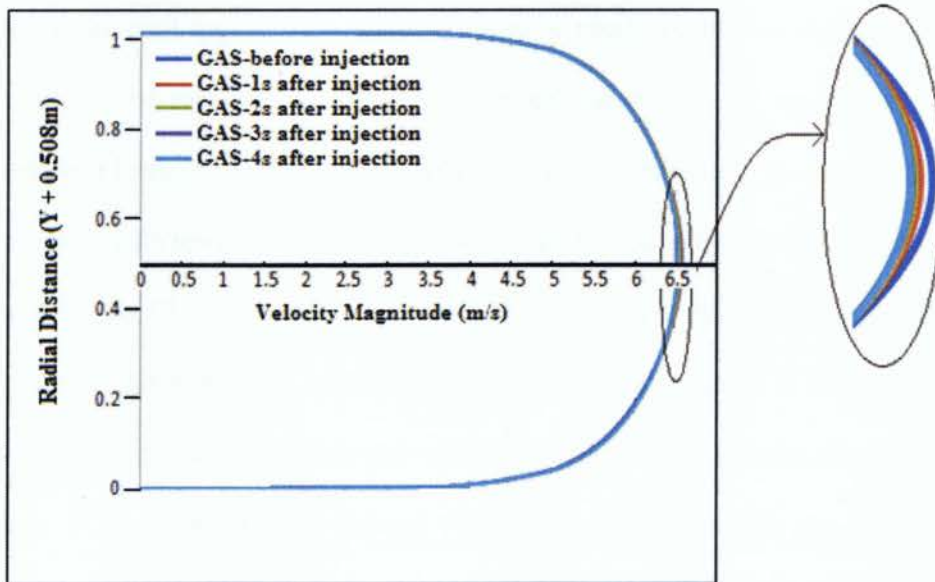


Figure 4.6 Velocity profiles of the gas just before and 4 seconds after injection of particles at every segment of pipeline from injection point to the outlet.

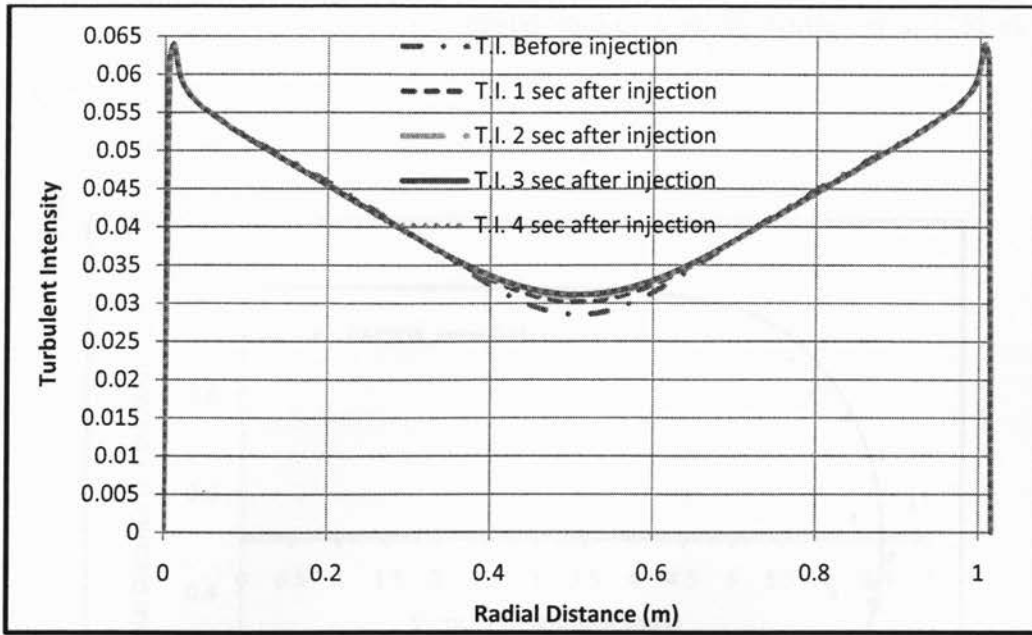


Figure 4.7 Stream wise turbulent intensity profile of gas before and within 4 seconds of particle injection. The values at each time are correspondent to every segment of the pipeline from injection point to the outlet.

As Figure 4.7 illustrates, the turbulent intensity of the gas flow reaches its maximum near the wall region. Indeed increase of turbulent intensity is in accordance with the decrease of mean velocity toward the wall region. However, it should be remembered that the turbulent intensity approaches zero at the sub layer very close to the wall where flow is essentially laminar. The results of turbulent intensity profile and velocity profile of the turbulent gas flow in this study are in good agreement with results of solid-gas flow simulations done by Lun [35]. Figure 4.8 shows both gas velocity profile and particles at the outlet 4 seconds after injection and Figure 4.9 illustrates the size distribution of corresponding particles with respect to their radial distance. The highest velocity magnitude is $\sim 6.9\text{m/s}$ which is achieved by particles positioned 0.6 m in radial distance from the bed and the lowest velocity corresponds to the one positioned on the pipe bed. It can be seen that particles in the core region are slightly faster than the gas. That is usually the case for particles with sizes as small as $1\ \mu\text{m}$ and the gas Reynolds number of about

4×10^5 which is in agreement with experimental studies done by Kulick et al [25] as well as numerical study by Lun [35].

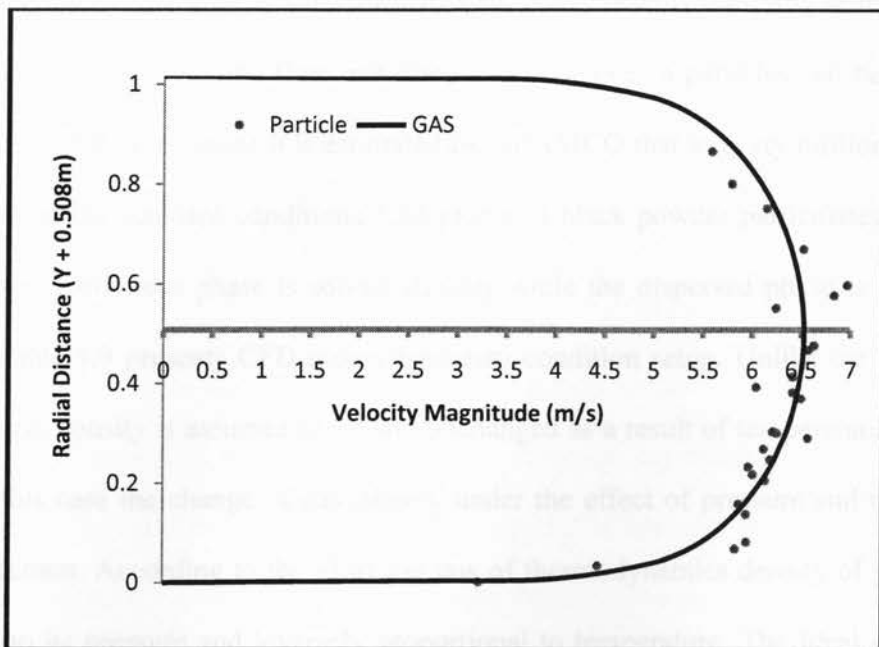


Figure 4.8 Velocity profiles of the gas and particles at the outlet 4 s after injection

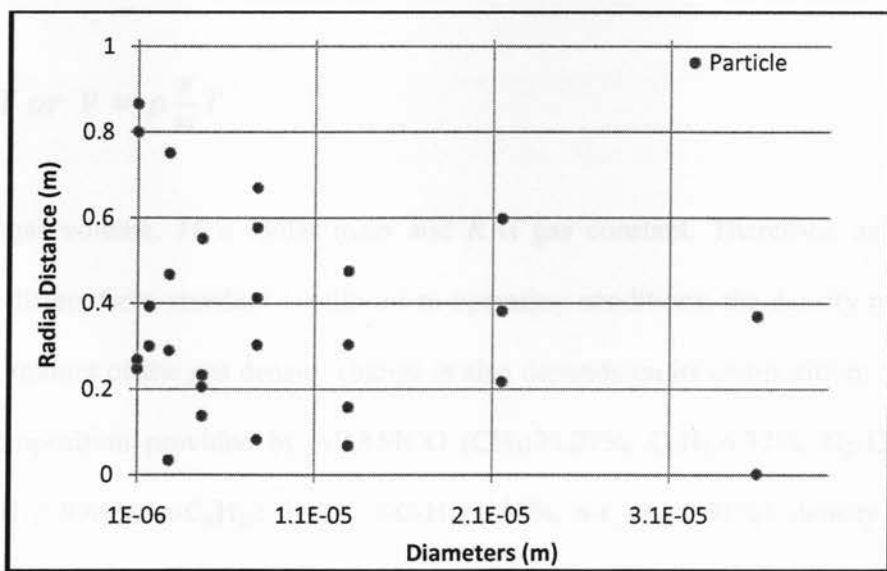


Figure 4.9 Distribution of particles size at the outlet vs. particles radial distance from pipe bed

4.3.2 Continuous Injection of 25 μm Particles

The second case study is simulation of particles with constant size of 25 μm , continuously injected into the gas flow at the inlet surface. Table 4.7 presents the particle injection setup. Based on the known gas volume flow rate, the mass flow rate of particles can be computed as approximately 0.0192 gm/s since it is estimated by ARAMCO that in every million cubic feet of sales gas flow at the standard conditions 1.84 grams of black powder particulates exist. In this case study, the continuous phase is solved steadily while the dispersed phase is being tracked unsteadily. Table 4.9 presents CFD model boundary condition setup. Unlike the previous case study where gas density is assumed to remain unchanged as a result of temperature and pressure changes, in this case the change of gas density under the effect of pressure and temperature is taken into account. According to the ideal gas law of thermodynamics density of gas is directly proportional to its pressure and inversely proportional to temperature. The Ideal gas law is the equation of state of a hypothetical ideal gas. It is a good approximation to the behavior of gases under various conditions and can be written as

$$PV = \frac{m}{M}RT \text{ or } P = \rho \frac{R}{M}T \quad (4.1)$$

where V is gas volume, M is molar mass and R is gas constant. Therefore, as pressure and temperature differs from standard conditions to operating conditions, the density of the gas also differs. The amount of the gas density change is also depends on its composition. According to sales gas composition provided by ARAMCO (CH_3 :75.27%, C_2H_6 :6.32%, N_2 :13.84%, C_3H_8 : 2.50%, $i\text{-C}_4\text{H}_{10}$: 0.49%, $n\text{-C}_4\text{H}_{10}$: 0.93%, $i\text{-C}_5\text{H}_{12}$:0.33%, $n\text{-C}_5\text{H}_{12}$:0.31%), density of gas under operating pressure and temperature of respectively 900 psi and 316 $^\circ\text{K}$ is computed as about 61.8

Kg/m^3 , using HYSIS software. Table 4.8 presents characteristics of the gas flow under operating condition at the injection point. By comparing velocity profiles of gas shown by Figures 4.3 and 4.12 it can be noticed that the mean velocity of gas along the pipeline is slightly lower in case where density of gas is considered 61.8 Kg/m^3 . In fact, the difference in results of velocity profile between this case study and previous case study is due to different density values used in each case. Figure 4.10 illustrates graphical simulation of particles along the pipeline and Figure 4.11 shows age of corresponding particles from the time of their injection into gas flow. By looking at Figure 4.10, it can be noticed that after about 7m from the injection point particles begin to trip away from the pipe's upper wall due to gravity. Since all particles are of the same size, the effect of gravity is consistently uniform. However, depending on particles' angle of orientation and their radial position in the gas flow, particles tendency to move toward the pipe bed varies. For instance, particles moving in the core region of the gas flow are less likely to sink before they reach the outlet. In comparison, most of particles moving in the lower bound of core region are gradually being shifted toward the bed and roll toward the outlet with lower velocity magnitudes ranging between 3.5 m/s to 4.5 m/s. All particles eventually make it to the outlet but at different times. For example, particles from the earliest injection will reach the outlet at the earliest time of about 4 sec and latest time of about 7 sec. That is illustrated by Figure 4.11. Since the distribution of particles is uniform, the concentration of particles rolling over the pipeline bed is linearly increasing from inlet to outlet, as shown by Figure 4.15. It can be seen that particles' concentration reaches a maximum amount of about 0.26 gram per cubic meter volume of gas near the pipeline outlet.

Table 4.6 Particle properties

<i>Material</i>	<i>Black Powder-Magnetite-Fe₃O₄</i>
<i>Density (Kg/m³)</i>	<i>5150</i>
<i>Specific gravity</i>	<i>5.15</i>
<i>Diameter (μm)</i>	<i>25</i>
<i>Shape</i>	<i>Sphere</i>

Table 4.7 Particle injection setup

<i>Injection Type</i>	<i>Surface</i>
<i>Injection Angle</i>	<i>Face normal direction</i>
<i>Injection Duration (s)</i>	<i>Continuous</i>
<i>Initial Velocity of the particles at the injection point (m/s)</i>	<i>0</i>
<i>Distribution</i>	<i>Uniform</i>
<i>Turbulent Dispersion of particles</i>	<i>Stochastic tracking</i>
<i>Tracking Particles</i>	<i>Un-steady</i>
<i>Mass Flow Rate of Particles (gm/s)</i>	<i>0.0192</i>

Table 4.8 Characteristics of the gas flow at the injection point at operating conditions

<i>Volume Flow Rate (m³/s)</i>	<i>5.257</i>
<i>Volume Flow Rate (mmcf/d)</i>	<i>16</i>
<i>Velocity (v) (m/s)</i>	<i>6.49</i>
<i>Reynolds number</i>	<i>30,639,056</i>
<i>Pressure (psi)</i>	<i>900</i>
<i>Temperature (Kelvin)</i>	<i>316</i>
<i>Density (kg/m³)</i>	<i>61.8</i>
<i>Viscosity Kg/m-s (μ)</i>	<i>0.0000133</i>

Table 4.9 CFD model boundary condition setup

<i>Model</i>	<i>2D-inlet-wall-outlet</i>
<i>Solver</i>	<i>Pressure based, Steady, Superficial Velocity</i>
<i>Inlet</i>	<i>Velocity inlet-Fully developed flow</i>
<i>Outlet</i>	<i>Pressure Outlet</i>
<i>Viscous Model</i>	<i>Standard-k-ε (2eq)</i>
<i>Turbulent Specification Method</i>	<i>Intensity and Hydraulic Diameter</i>

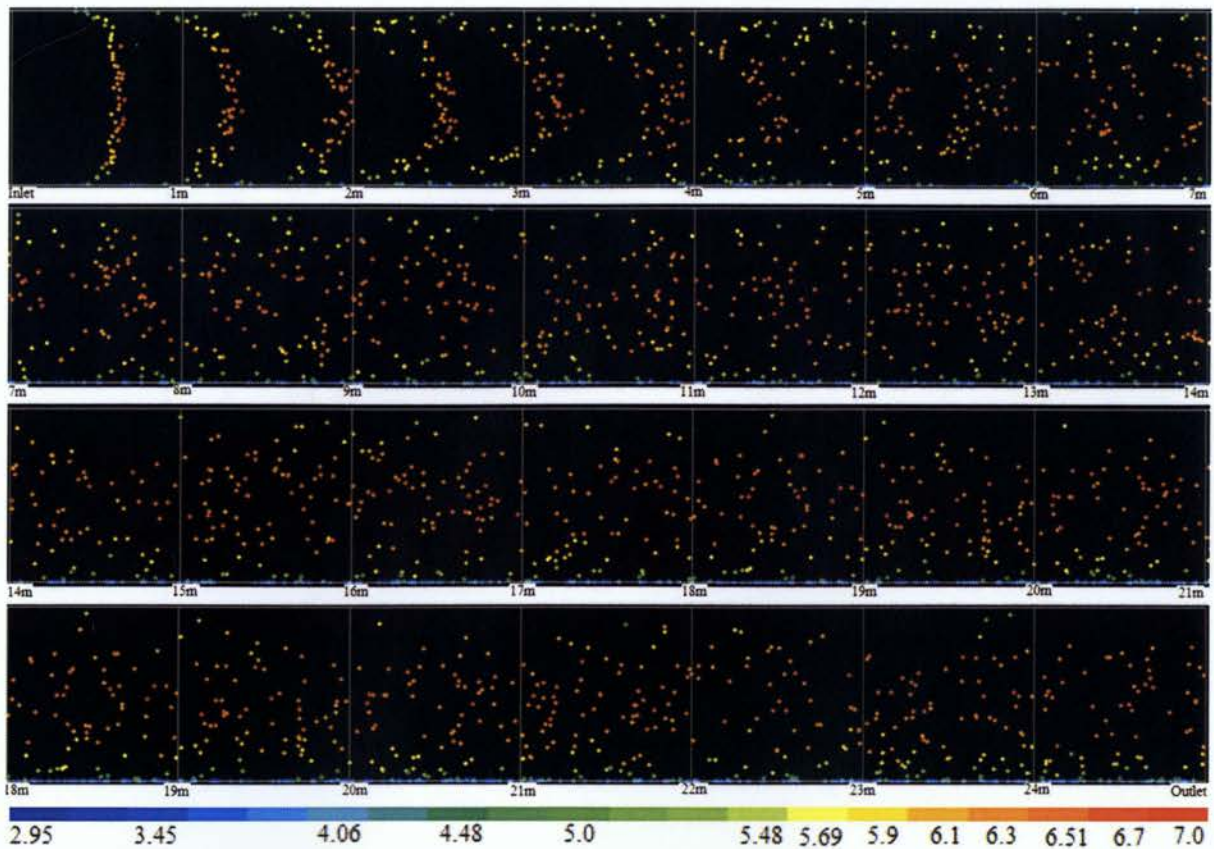


Figure 4.10 Graphical tracking of black powders particulates, carried by fully developed gas flow, from injection point to the outlet. Colored by velocity magnitude (m/s)

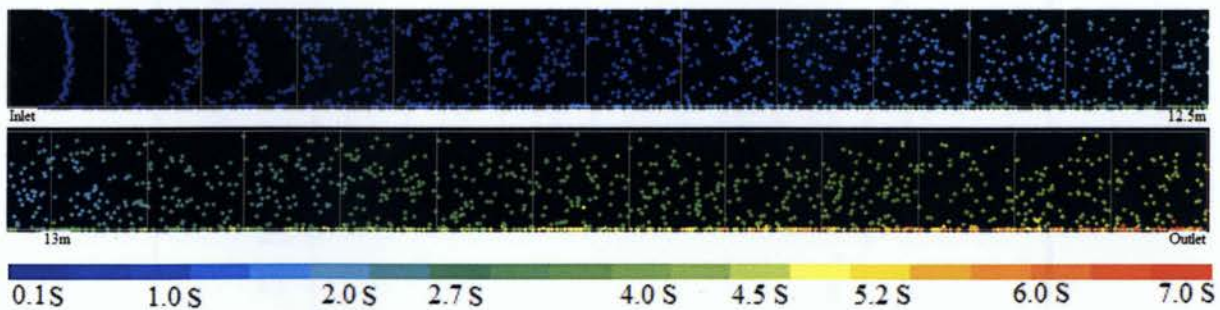


Figure 4.11 Graphical tracking of black powders particulates. Colored by particle residence time (Age of particle since their injection into gas flow) (second)

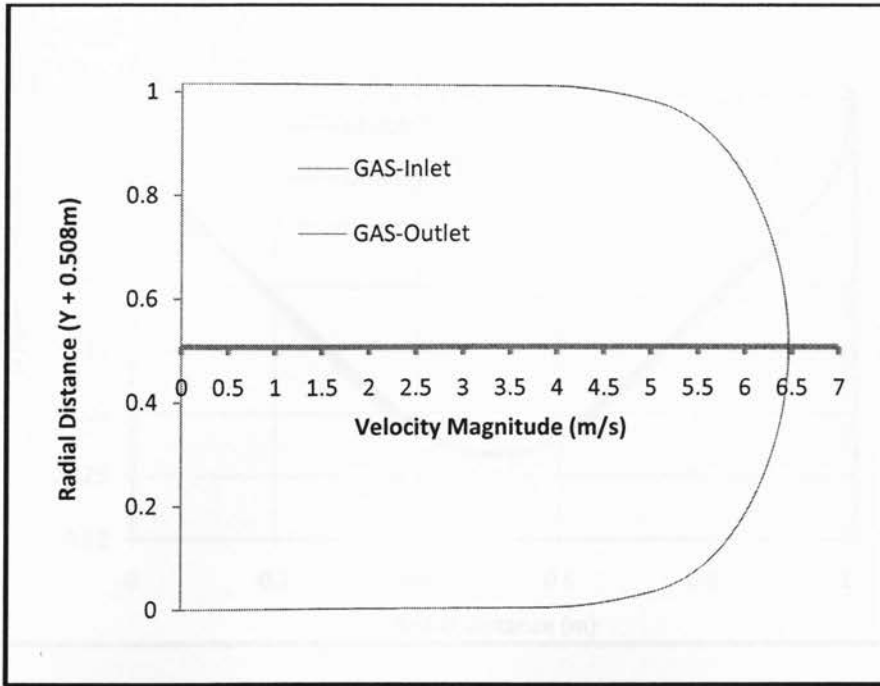


Figure 4.12 Velocity profile of gas at inlet and outlet during particle injection

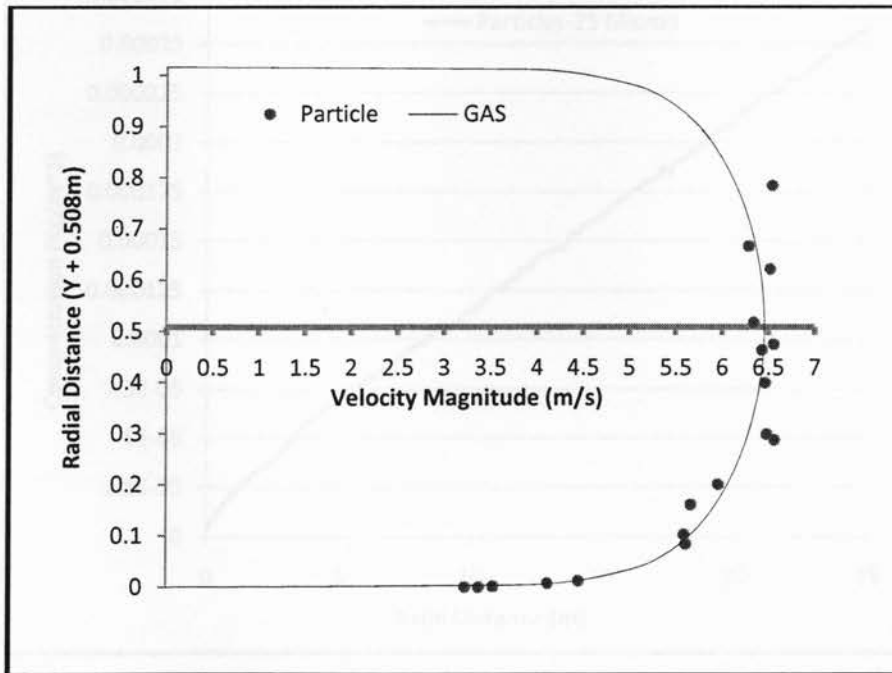


Figure 4.13 Velocity profiles of gas and 25µm particles at the pipeline outlet

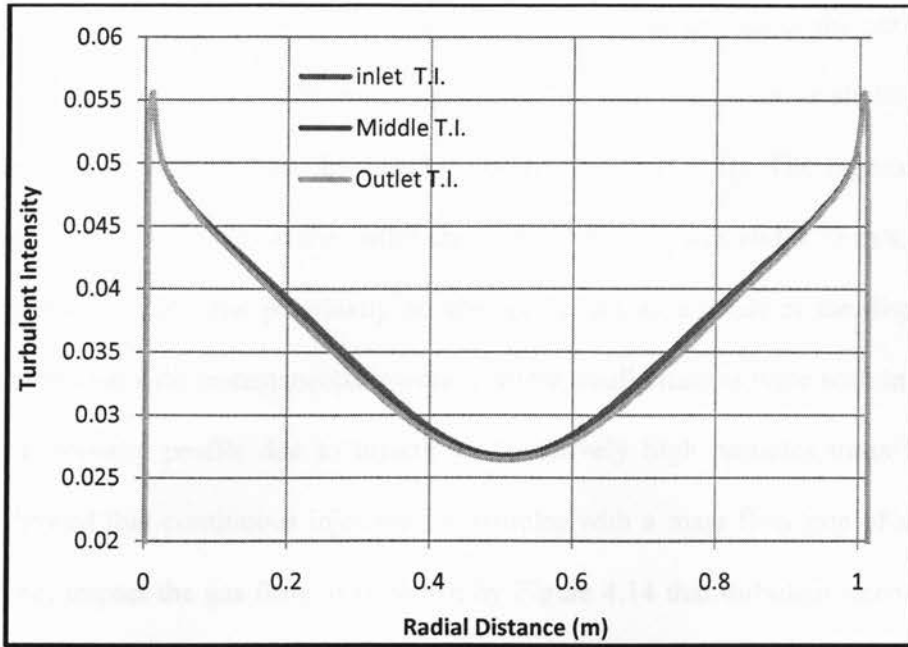


Figure 4.14 Stream wise turbulent intensity profile of gas at the inlet, middle and outlet of the pipeline

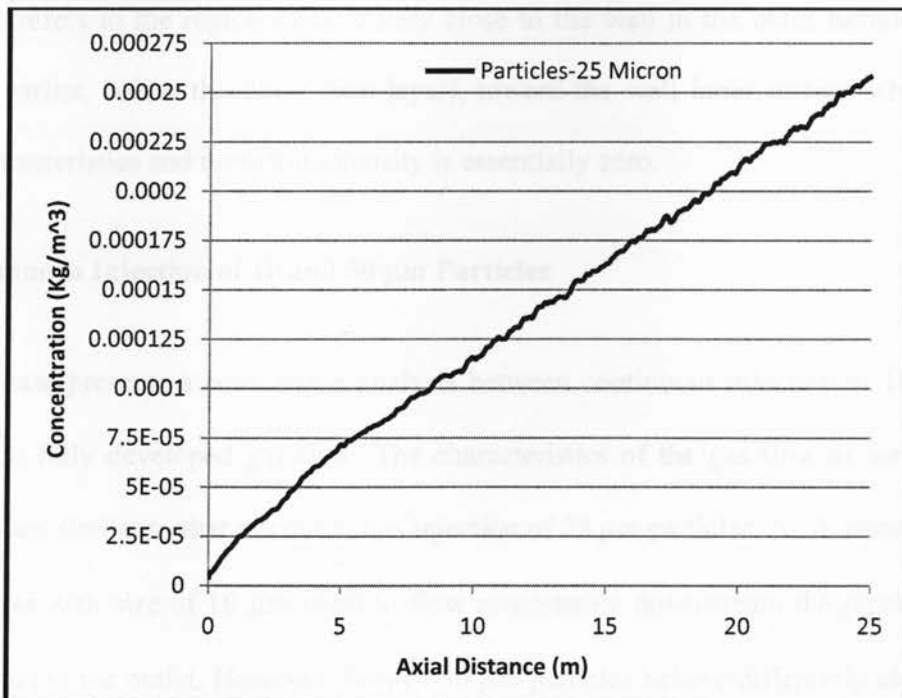


Figure 4.15 Concentration of particles along the pipeline bed in terms of particles mass per unit volume

Figure 4.13 illustrates particles' positioning and their velocity magnitude at the outlet as well as the gas velocity profile. As expected, most particles in the core region move slightly faster than the gas (This was also emphasized by Lun [35] & Kulick et al [25]). The highest and lowest velocity magnitudes of particles at the outlet are respectively 6.52m/s and 3.25 m/s. Simulations of the gas profile indicate that practically no change occurs as a result of the dispersed phase flow. Unlike the case with instantaneous injection where small changes were seen in gas velocity and turbulent intensity profile due to injection of relatively high particles mass loading, this study case showed that continuous injection of particles with a mass flow rate of about 0.0192 gm/s would not impact the gas flow. It is shown by Figure 4.14 that turbulent intensity of gas is generally consistent along the pipeline. In fact, turbulent intensities in the gas flow from the core region to the near wall region vary from approximately 2.7 % to 5.5%. Similar to the previous case, the highest intensity occurs near the wall region where mean velocity is lowest. The near wall region refers to the region of flow very close to the wall in the outer turbulent layer. As mentioned earlier, below this layer (sub layer), toward the wall inner surface where flow has laminar characteristics and turbulent intensity is essentially zero.

4.3.3 Continuous Injection of 10 and 50 μm Particles

This study case presents a comparison analysis between continuous injection of 10 and 50 μm particles into fully developed gas flow. The characteristics of the gas flow as well as particle distribution are similar to that of continuous injection of 25 μm particles. As illustrated by Figure 4.16, particles with size of 10 μm seem to flow consistently downstream the pipeline from the injection point to the outlet. However, flow of 50 μm particles behave differently along the pipe. That is more noticeable almost after the mid segment of the pipeline where particles tend toward

the pipeline bed. Indeed since the characteristic of carrier phase is the same, this simulation is reasonable considering the fact that gravity is more effective on larger size particles.

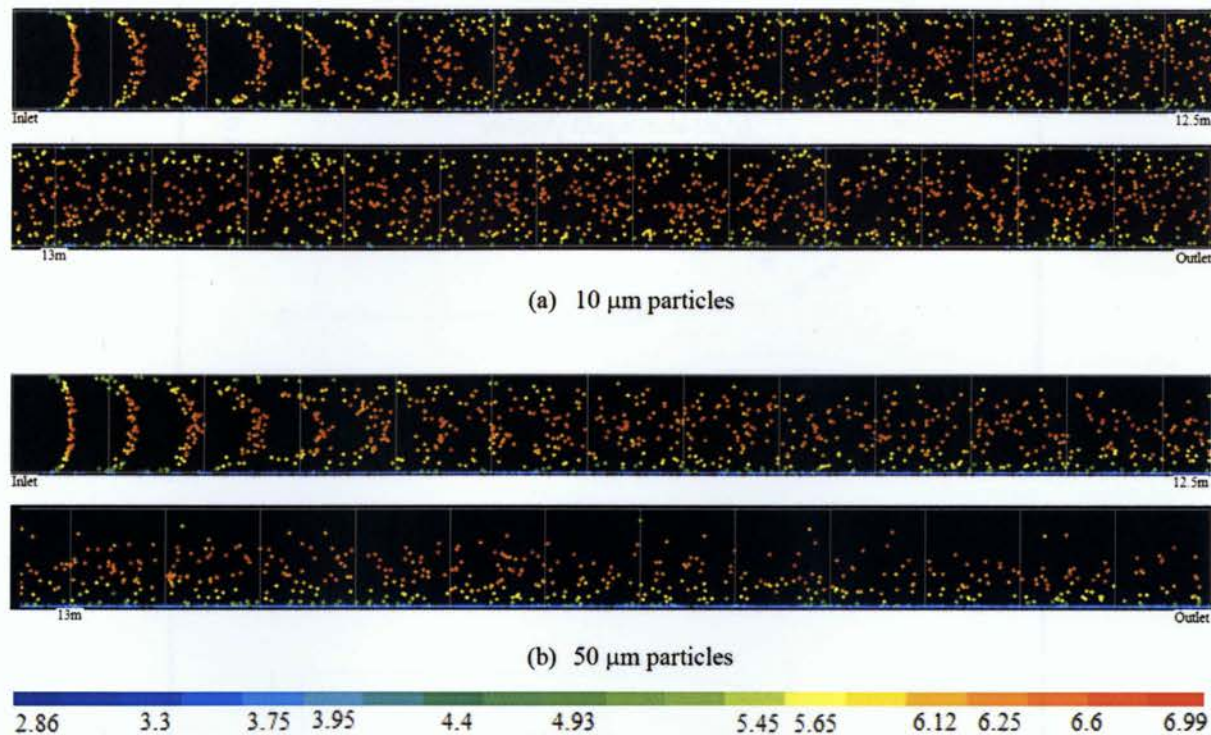


Figure 4.16 Graphical tracking of black powder particulates, carried by fully developed gas flow, from injection point to the outlet for (a) particles with diameters of 10 μm and (b) particles with diameters of 50 μm. Colored by velocity magnitude (m/s)

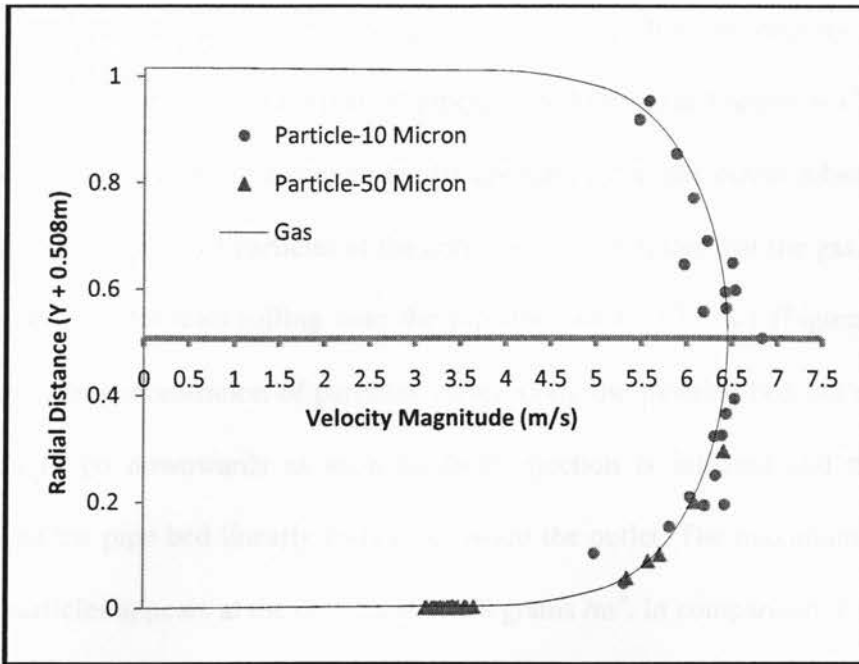


Figure 4.17 Velocity profiles of gas and particles at the pipeline outlet.

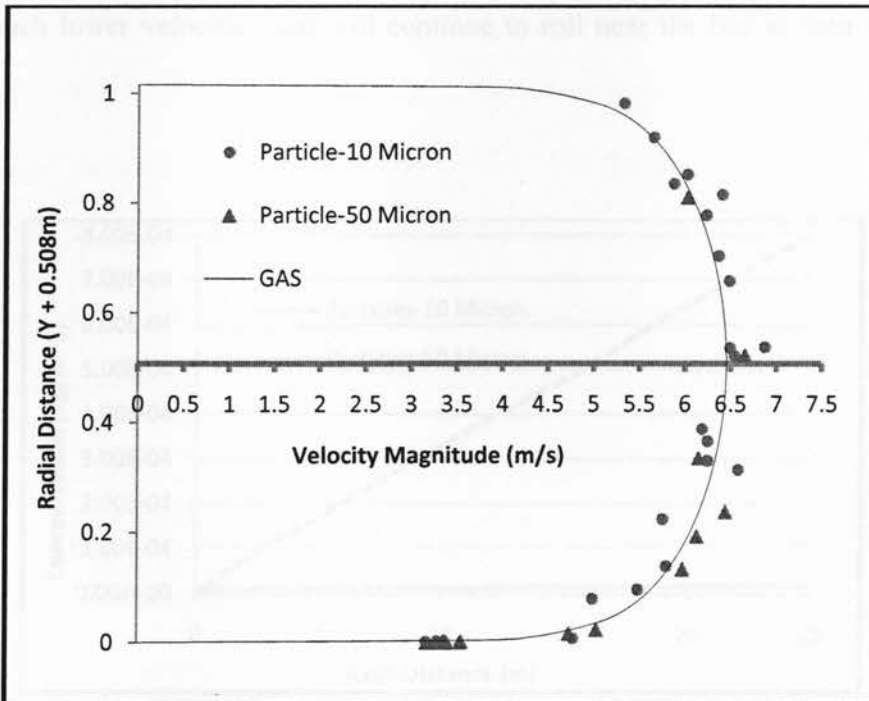


Figure 4.18 Velocity profiles of gas and particles at the pipeline middle.

The velocity magnitude of 10 and 50 μm particles as well as the gas velocity profile can be carefully studied at the middle and outlet of pipeline by looking at Figures 4.17 and 4.18. As illustrated, maximum velocity is achieved by 10 μm particle at the outlet which is ~ 6.9 m/s. Similar to previous cases, most particles at the core region flow faster than the gas. However, the maximum velocity of particles rolling over the pipeline bed is 3.73 m/s (Figure 4.17). Figure 4.19 shows how the concentration of particles varies along the pipeline bed. As shown, 50 μm particles begin to go downwards as soon as their injection is initiated and thereafter their concentration on the pipe bed linearly increases toward the outlet. The maximum concentration of the 50 μm particles appears at the outlet and is 0.8 grams /m³. In comparison, concentration of 10 μm particles over the pipe bed is nearly constant from inlet to the outlet. Since particle's injection is implemented from the entire surface of the injection point, it can be imagined that in case of 10 μm , those particles injected near the pipe bed will be carried by their surrounding gas flow with much lower velocities and will continue to roll near the bed at their original radial distance.

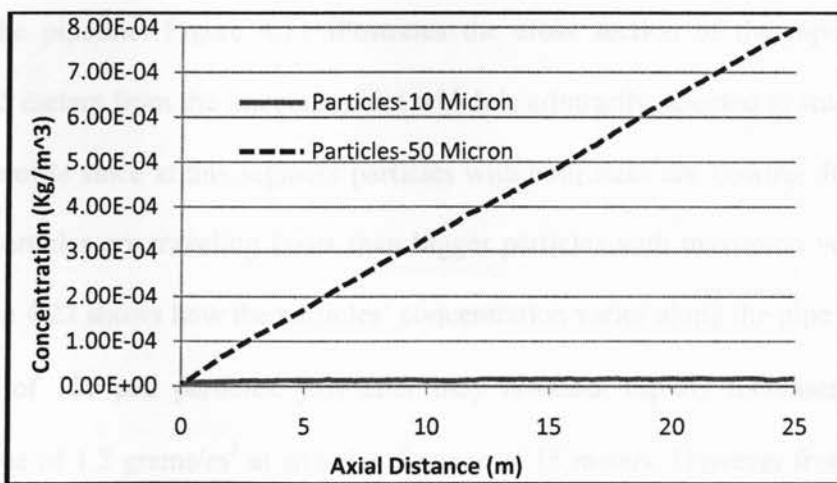


Figure 4.19 Concentration of particles along the pipeline bed in terms of particles mass per unit volume

In fact, gas with maximum velocity of 6.49 m/s, corresponding to 900 mmscfd (16 mmcfd), would carry away almost all the 10 μm particles as it progress along the pipeline but not the ones five times bigger. In the case of 50 μm particles, it seems that the above volumetric flow rate of gas cannot provide enough lift force to keep particulates suspended in the flow. So, even those released at higher radial distance would eventually fall down the flow and since the carrier flow is consistent and continuous their appearance along the pipe bed increases linearly. That is in accordance with Smart [14] studies, where the required volume flow rate and velocity of gas to move particulates in sales gas pipelines were experimentally examined with respect to pipeline diameters and size of particles.

4.3.4 Continuous Injection of 75 and 150 μm Particles

This study case is similar to the previous case; however, comparison is conducted for particles having sizes of 75 and 150 μm . As shown by Figure 4.20, no particles appear at the cross section of pipe outlet. In fact both 75 and 150 μm particles sink to the bed by the time they reach the outlet, although almost all the particles having a size of 150 μm are sinking nearly at the middle segment of the pipeline. Figure 4.21 illustrates the cross section of the pipeline with axial distance of 6.5 meters from the injection point which is arbitrarily selected to study particles and gas velocity profile since at this segment particles with both sizes are flowing. It can be noticed that smaller particles are traveling faster than bigger particles with maximum velocity of about 6.7 m/s. Figure 4.22 shows how the particles' concentration varies along the pipe bed. As shown, concentration of 150 μm particles, just after they released, rapidly increases and reach its maximum value of 1.2 grams/m^3 at an axial distance of 15 meters. However from that point the concentration remains constant all the way to the outlet.

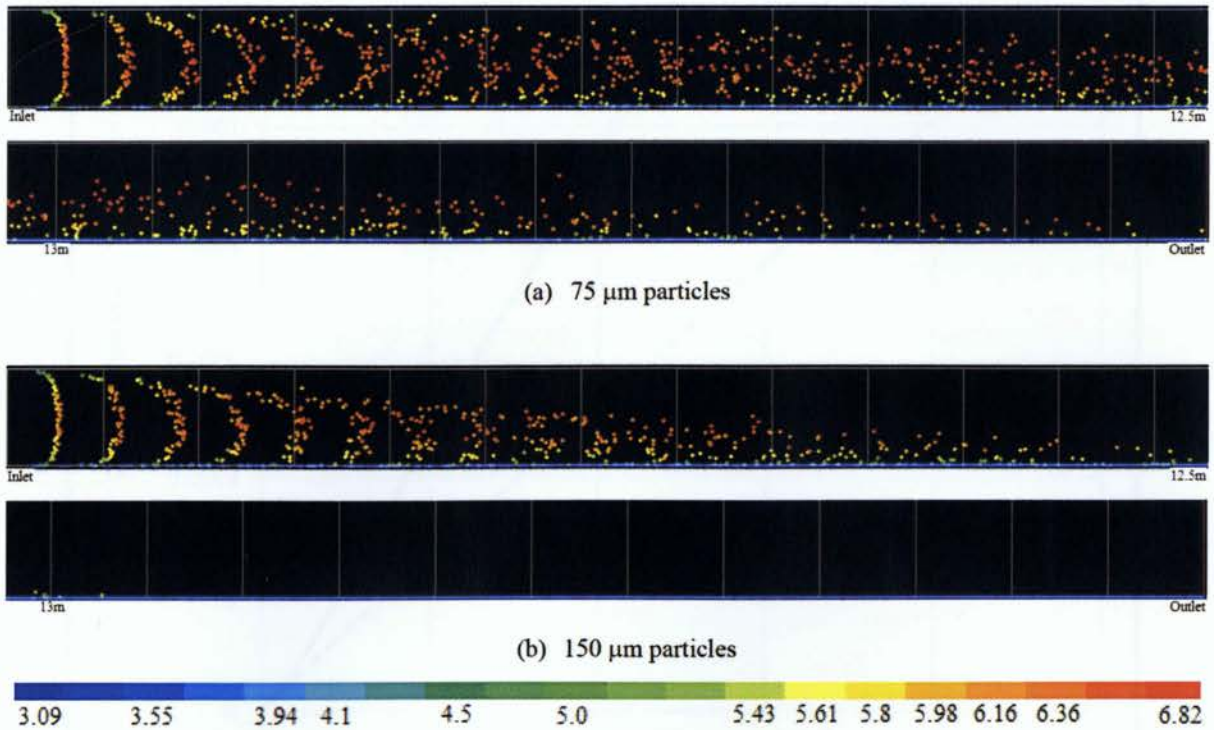


Figure 4.20 Graphical tracking of black powders particulates, carried by fully developed gas flow, from injection point to the outlet for (a) particles with diameters of 75 μm and (b) particles with diameters of 150 μm . Colored by velocity magnitude (m/s)

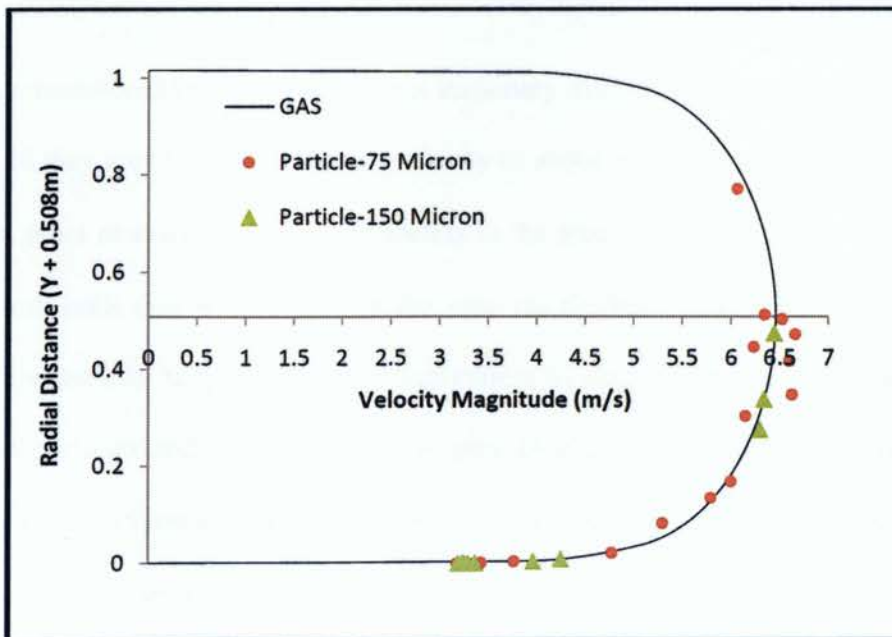


Figure 4.21 Velocity profiles of gas and particles at axial distance of 6.5m from the injection point

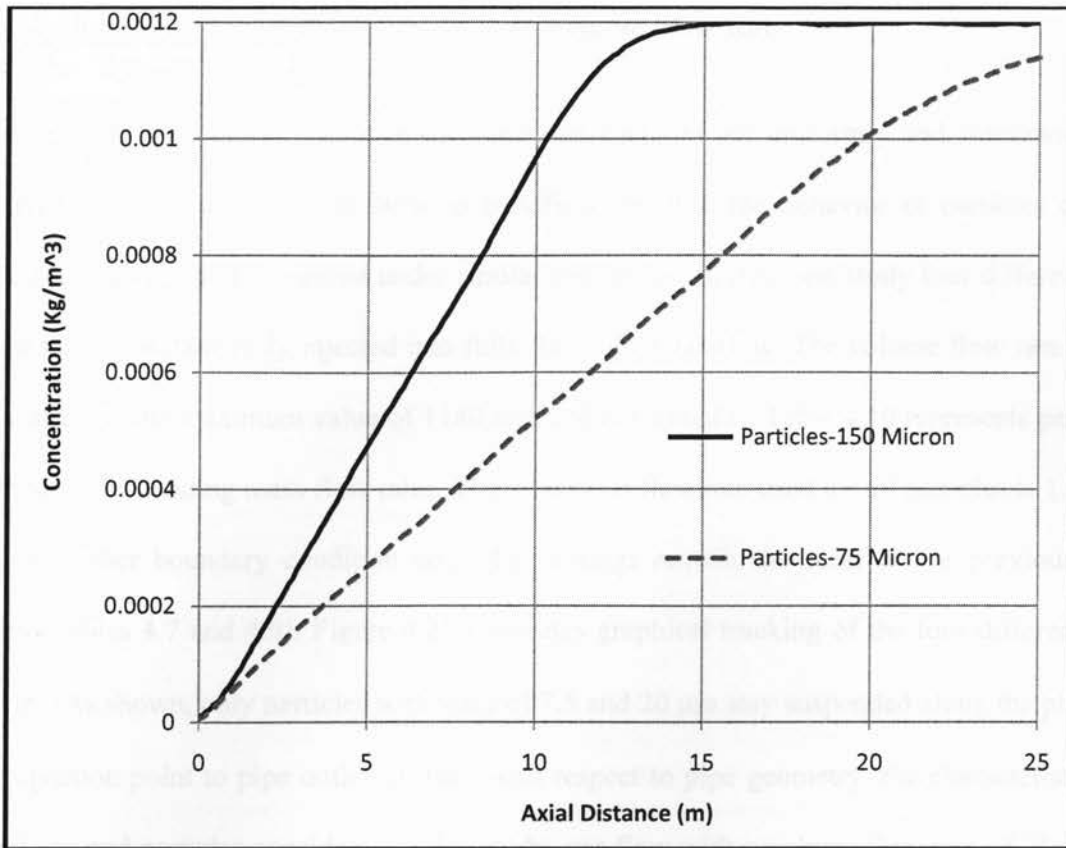


Figure 4.22 Concentration of particles along the pipeline bed in terms of particles mass per unit volume

It should be remembered that particles are not stationary over the pipeline bed and as illustrated by Figure 4.20 they move with a minimum velocity of about 3 m/s. Therefore, it can be assumed that from the point at axial distance of 15 meters to the pipe outlet, 150 μm particles are neatly line up and roll until they eventually exit the pipe via the bed surface. However, if for some reason the pipeline bed happened to have unevenness in some segments, it would prevent the movement of particles and eventually lead to pipe blockage over time. Similarly this would become the case for 75 μm particles if the pipe's length was longer since almost all of them sink to the bed by the time they reach the outlet.

4.3.5 Multiple Injections with Maximum Gas Volume Flow Rate

Studying particle-gas flow, in which different size particles are uniformly and simultaneously injected into the continuous gas flow, is beneficial because the behavior of particles can be predicted, analyzed and compared under similar conditions. In this case study four different size particles are simultaneously injected into fully developed gas flow. The volume flow rate of the gas is taken as the maximum value of 1180 mmscfd (21 mmcfd). Table 4.10 represents particles and their corresponding mass flow rates. The total mass flow rate used for all particles is 1.97E-5 Kg/s. All other boundary condition and CFD settings remain the same as for previous case studies (Tables 4.7 and 4.9). Figure 4.23 illustrates graphical tracking of the four different size particles. As shown, only particles with sizes of 7.5 and 20 μm stay suspended along the pipeline from injection point to pipe outlet. In fact, with respect to pipe geometry, the characteristics of natural gas and particles considered in this study, gas flow with a volume flow rate of 21mmcfd ($6.9 \text{ m}^3/\text{s}$) creates enough lift and drag forces so that particles with size of 20 μm or less can be flowing downstream the pipeline until they exit the pipe without sinking over the pipe bed as a consequence of the gravity force. However, as illustrated by Figure 4.23 (d), the gas volume flow rate cannot create sufficient lift force to keep particles having the size of 150 μm to remain suspended in the gas medium all the way to the pipeline outlet.

Figures 24 and 25 respectively show the velocity profiles of gas and particles at the outlet and middle of the pipeline. It is illustrated that most of the particles are traveling faster than the gas at the outlet and the highest velocity is about 9 m/s which is achieved by 7.5 μm particles at a radial distance of approximately 0.36 m. The average velocity of floating particles at the outlet is roughly 3% faster than the gas velocity. However, most particles at the middle are flowing with

same velocity as the gas. Considering the gas velocity profile at the middle and outlet, it can be seen that the flow of gas has not been affected by multi dispersion of particles for the specified mass flow rate as flow progress from middle to the outlet. That is in comparison with the first study case which showed how instantaneous injection of relatively high mass loading particles would impact gas flow profile.

Table 4.10 Particles size and mass flow rate

<i>Diameter (μm)</i>	<i>Mass Flow Rate (Kg/s)</i>
7.5	1.80E-5
20	9.60E-7
75	2.40E-7
150	4.80E-7

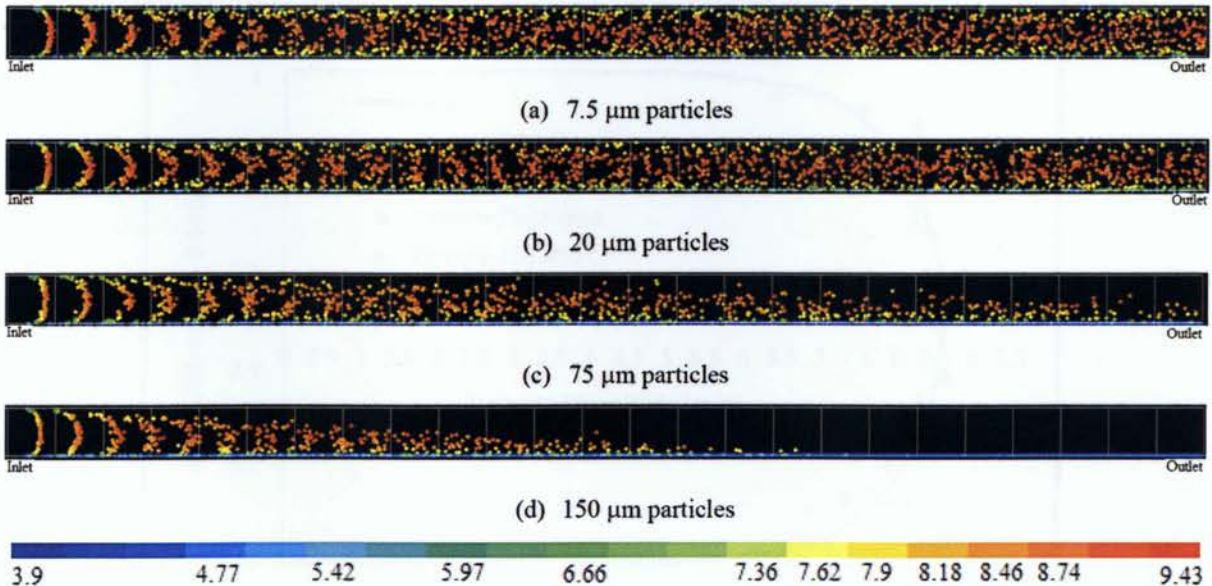


Figure 4.23 Graphical tracking of multiple injections of black powders particulates, carried by fully developed gas flow, from injection point to the outlet for different sized particles. Colored by velocity magnitude (m/s)

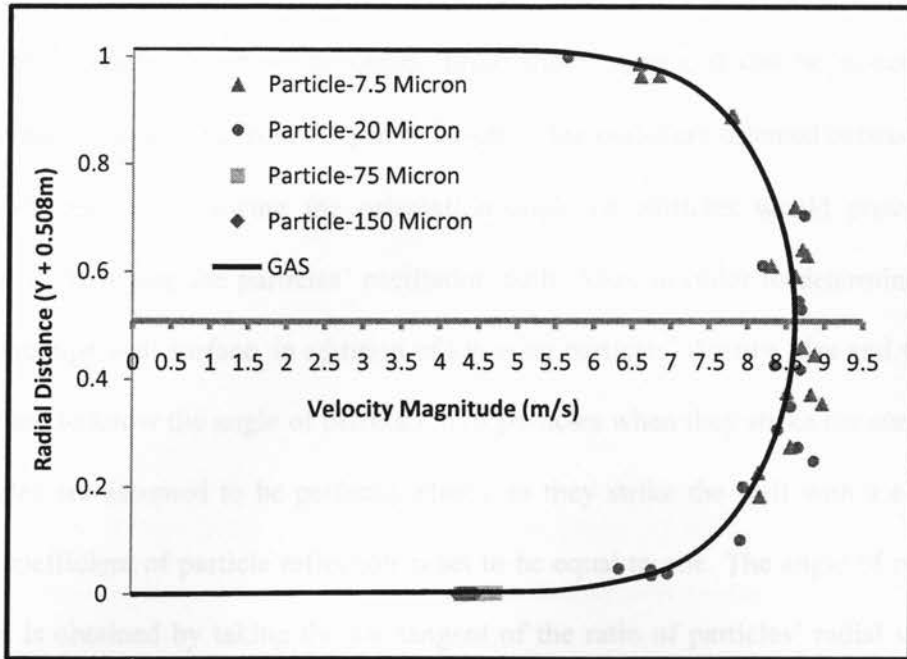


Figure 4.24 Velocity profiles of gas and particles at the pipeline outlet

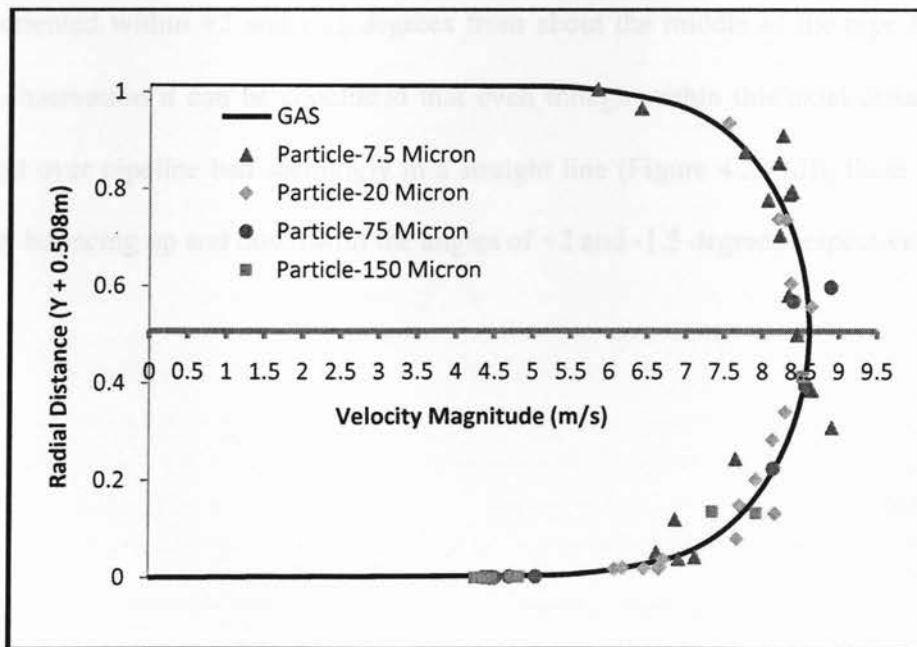


Figure 4.25 Velocity profiles of gas and particles at the pipeline middle

Figures 4.26 & 4.27 illustrate particles' angle of orientation with respect to their velocity magnitude and radial position at the outlet. From these figures, it can be noticed that most particles having sizes ranging from $7.5 \mu\text{m}$ to $20 \mu\text{m}$ at the outlet are oriented between the angles of $+3$ and -3 degrees. Knowing the orientation angle of particles would provide valuable information in predicting the particles' oscillation path. Also, in order to determine the rate of erosion on the pipe wall surface, in addition of knowing particles' density, size and velocity, it is quite important to know the angle of orientation of particles when they strike the surface. In this study particles are assumed to be perfectly elastic as they strike the wall with a certain angle. Hence, the coefficient of particle reflection is set to be equal to one. The angle of orientation of the particles is obtained by taking the arc tangent of the ratio of particles' radial velocity over particles axial velocity. Since the velocity of the particles varies within the same range from the injection point to the outlet, it can be reasonably assumed that particles would be oriented within the angles of $+3$ and -3 degrees along the pipeline. However, particles having the size of $150 \mu\text{m}$ would be oriented within $+2$ and -1.5 degrees from about the middle of the pipe to the outlet. From this observation it can be concluded that even though within this axial distance $150 \mu\text{m}$ particles roll over pipeline bed seemingly in a straight line (Figure 4.23 (d)), these particles are consistently bouncing up and down with the angles of $+2$ and -1.5 degrees respectively.

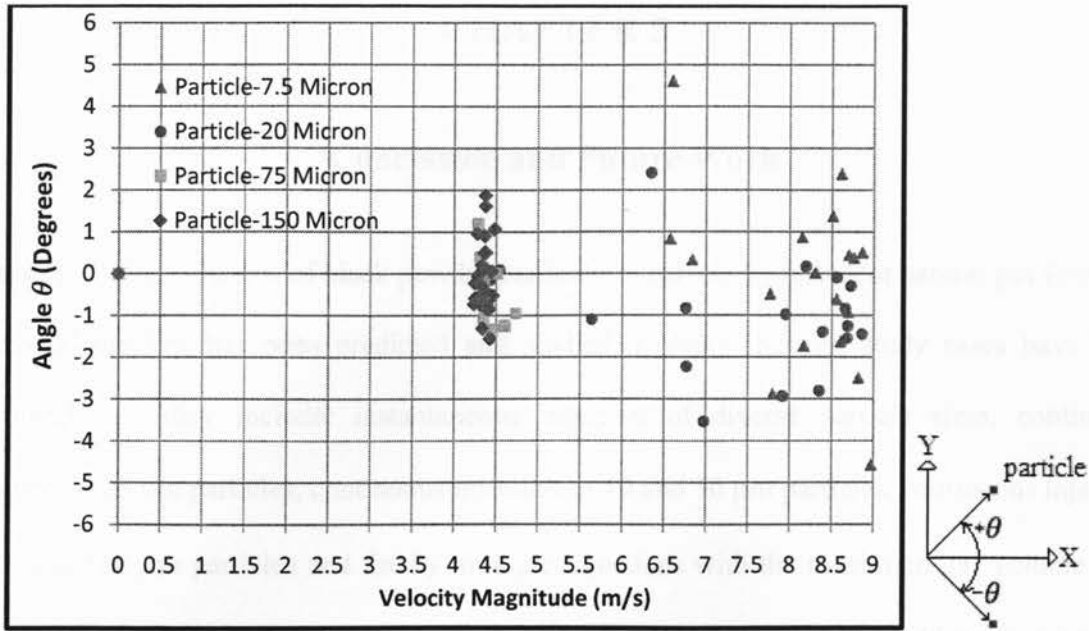


Figure 4.26 Velocity magnitudes of particles at the outlet vs. particles angle of orientation

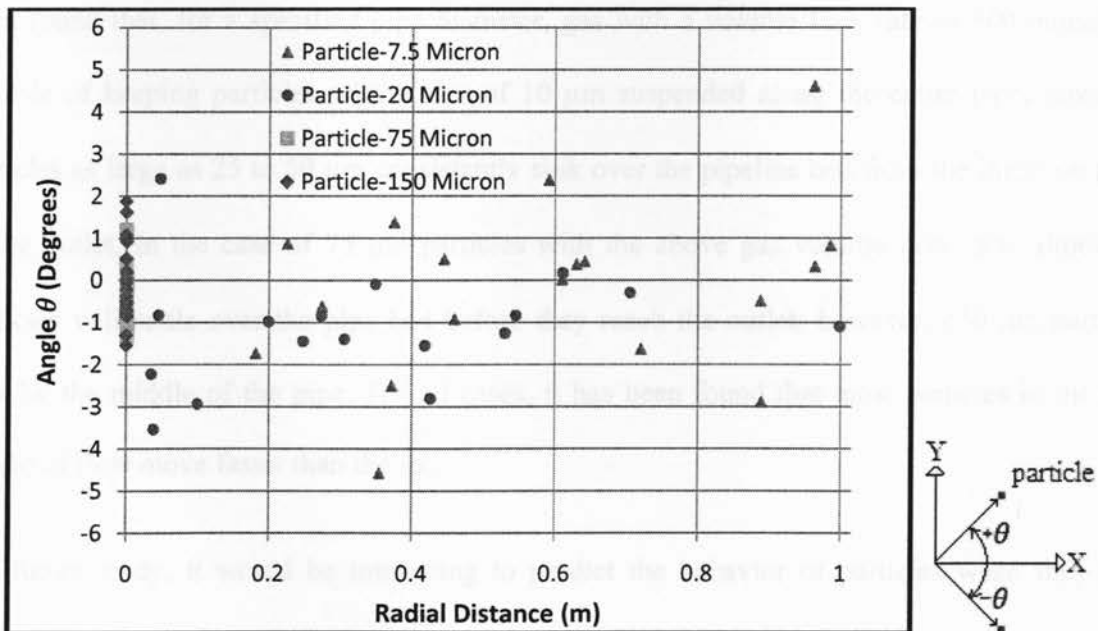


Figure 4.27 Radial distance of particles at the outlet vs. particles angle of orientation

CHAPTER 5

Conclusion and Future Work

In this thesis, the behavior of black powder particulates carried by turbulent natural gas flow in a horizontal pipeline has been predicted and studied in detail. Several study cases have been examined, and they include: instantaneous injection of diverse particle sizes, continuous injection of 25 μm particles, continuous injection of 10 and 50 μm particles, continuous injection of 75 and 150 μm particles and finally multiple injections with the maximum gas volume flow rate. For the case with instantaneous injection, it has been found that the sudden injection of a relatively high mass loading of particles, with specified density and size, into the fully developed gas flow would alter the flow profile in the core region and subsequently increase the turbulent intensity. For the cases with continuous injection of 10, 25, 50, 75 and 150 μm particles, it has been found that, for a specified pipe diameter, gas with a volume flow rate of 900 mmscfd is capable of keeping particles with a size of 10 μm suspended along the entire pipe; however, particles as large as 25 to 50 μm consistently sink over the pipeline bed from the injection point to the outlet. In the case of 75 μm particles with the above gas volume flow rate, almost all particles will settle over the pipe bed before they reach the outlet; however, 150 μm particles sink by the middle of the pipe. For all cases, it has been found that most particles in the core region of flow move faster than the gas.

For future study, it would be interesting to predict the behavior of particles when they pass through a valve or they reach a pipeline bend. Also, it would be interesting to study the erosion impact of the particles on the pipe.

APPENDIX

Input File for CFD Model Setup

A.1 Instantaneous Injection of Diverse Particle Sizes- Case Study

FLUENT

Version: 2d, dp, pbns, ske, unsteady (2d, double precision, pressure-based, standard k-epsilon, unsteady)

Models

Model	Settings
Space	2D
Time	Unsteady
Viscous	Standard k-epsilon turbulence model
Wall Treatment	Standard Wall Functions
Heat Transfer	Disabled
Solidification and Melting	Disabled
Species Transport	Disabled
Coupled Dispersed Phase	Enabled
Pollutants	Disabled
Pollutants	Disabled
Soot	Disabled

Boundary Conditions

Zones

Name	id	type
Gas	2	fluids
Wall	3	walls
Outlet	4	pressure-outlet
Inlet	5	velocity-inlet
Default-interior	7	interior

Wall

Condition	Value
Wall Motion	0
Define wall motion relative to adjacent cell zone?	Yes
Apply a rotational velocity to this wall?	No
Velocity Magnitude (m/s)	0
Define wall velocity components?	No
X-Component of Wall Translation (m/s)	0
Y-Component of Wall Translation (m/s)	0
Wall Roughness Height (m)	2.9999999e-05
Wall Roughness Constant	0.5
Discrete Phase BC Type	2
Normal	((polynomial angle 1))
Tangent	((polynomial angle 1))
Number of Splashed Drops	4

Material: steel (solid)

Property	Units	Method	Value(s)
Density	kg/m ³	constant	7833
Cp (Specific Heat)	J/kg-K	constant	871
Thermal Conductivity	W/m-K	constant	202.4

Solver Controls

Equation	Solved
Flow	Yes
Turbulence	Yes
Numeric	Enabled
Absolute Velocity Formulation	Yes

Unsteady Calculation Parameters

Time Step (s)	0.1
Max. Iterations per Time Step	40

Pressure-Velocity Coupling

Parameter	Value
Type	Coupled
Courant Number	200
Explicit Momentum Relaxation Factor	0.75
Explicit Pressure Relaxation Factor	0.75

Material Properties

Material: black-powder-magnetite (inert-particle)

Property	Units	Method	Value(s)
Density	kg/m ³	constant	5150
Cp (Specific Heat)	J/kg-K	constant	1680
Thermal Conductivity	W/m-K	constant	0.0454

Material: sales-gas (fluid)

Property	Units	Method	Value(s)
Density	kg/m ³	constant	0.80000001
Cp (Specific Heat)	J/kg-K	constant	1006.43
Thermal Conductivity	W/m-K	constant	0.0242
Viscosity	kg/m-s	constant	1.33e-05
Molecular Weight	kg/Kmol	constant	28.966

A.2 Continuous Injection of 10, 25, 50, 75 and 150 μm Particles- Case Study

FLUENT

Version: 2d, dp, pbns, ske (2d, double precision, pressure-based, standard k-epsilon)

Models

Model Settings

Space 2D

Time	Steady
Viscous	Standard k-epsilon turbulence model
Wall Treatment	Standard Wall Functions
Heat Transfer	Disabled
Solidification and Melting	Disabled
Species Transport	Disabled
Coupled Dispersed Phase	Enabled
Pollutants	Disabled
Pollutants	Disabled
Soot	Disabled

Boundary Conditions

Zones

name	id	type
gas	2	fluid
wall	3	wall
outlet	4	pressure-outlet
inlet	5	velocity-inlet
default-interior	7	interior

wall

Condition	Value
Wall Motion	0
Define wall motion relative to adjacent cell zone?	Yes
Apply a rotational velocity to this wall?	No
Velocity Magnitude (m/s)	0
Define wall velocity components?	No
X-Component of Wall Translation (m/s)	0
Y-Component of Wall Translation (m/s)	0
Wall Roughness Height (m)	2.9999999e-05
Wall Roughness Constant	0.5
Discrete Phase BC Type	2
Normal	((polynomial angle 1))
Tangent	((polynomial angle 1))
Number of Splashed Drops	4
Impact Angle Function	((polynomial angle 1))
Diameter Function	((polynomial 1.8e-09))

Velocity Exponent Function

((polynomial 0))

Solver Controls

Equations

Equation	Solved
Flow	Yes
Turbulence	Yes

Numerics

Numeric	Enabled
Absolute Velocity Formulation	Yes

Relaxation

Variable	Relaxation Factor
Density	1
Body Forces	1
Turbulent Kinetic Energy	0.80000001
Turbulent Dissipation Rate	0.80000001
Turbulent Viscosity	1
Discrete Phase Sources	0.5

Pressure-Velocity Coupling

Parameter	Value
Type	Coupled
Courant Number	200
Explicit Momentum Relaxation Factor	0.75
Explicit Pressure Relaxation Factor	0.75

Discretization Scheme

Variable	Scheme
Pressure	Standard

Momentum	Second Order Upwind
Turbulent Kinetic Energy	Second Order Upwind
Turbulent Dissipation Rate	Second Order Upwind

Material Properties

Material: black-powder-magnetite (inert-particle)

Property	Units	Method	Value(s)
Density	kg/m ³	constant	5150
Cp (Specific Heat)	J/kg-K	constant	1680
Thermal Conductivity	W/m-K	constant	0.0454

Material: sales-gas (fluid)

Property	Units	Method	Value(s)
Density	kg/m ³	constant	61.799999
Cp (Specific Heat)	J/kg-k	constant	1006.43
Thermal Conductivity	W/m-k	constant	0.0242
Viscosity	kg/m-s	constant	1.33e-05
Molecular Weight	kg/Kmol	constant	28.966
Reference Temperature	K	constant	316

Material: steel (solid)

Property	Units	Method	Value(s)
Density	kg/m ³	constant	7833
Cp (Specific Heat)	J/kg-K	constant	871
Thermal Conductivity	W/m-K	constant	202.4

A.3 Multiple Injections with Maximum Gas Volume Flow Rate- Case Study

FLUENT

Version: 2d, dp, pbns, ske (2d, double precision, pressure-based, standard k-epsilon)

Models

Model	Settings
Space	2D
Time	Steady
Viscous	Standard k-epsilon turbulence model
Wall Treatment	Standard Wall Functions
Heat Transfer	Disabled
Solidification and Melting	Disabled
Species Transport	Disabled
Coupled Dispersed Phase	Enabled
Pollutants	Disabled
Pollutants	Disabled
Soot	Disabled

Boundary Conditions

Zones

name	id	type
gas	2	fluid
outlet	4	outflow
wall	3	wall
inlet	5	velocity-inlet
default-interior	7	interior

wall

Condition	Value
Wall Motion	0
Define wall motion relative to adjacent cell zone?	Yes
Apply a rotational velocity to this wall?	No
Velocity Magnitude (m/s)	0
Define wall velocity components?	No
X-Component of Wall Translation (m/s)	0
Y-Component of Wall Translation (m/s)	0
Wall Roughness Height (m)	2.9999999e-05
Wall Roughness Constant	0.5
Discrete Phase BC Type	2
Normal	((polynomial angle 1))
Tangent	((polynomial angle 1))
Number of Splashed Drops	4
Impact Angle Function	((polynomial angle 1))
Diameter Function	((polynomial 1.8e-09))

Solver Controls

Equations

Equation	Solved
Flow	Yes
Turbulence	Yes
Numeric	Enabled
Absolute Velocity Formulation	Yes

Linear Solver

Pressure-Velocity Coupling

Parameter	Value
Type	Coupled
Courant Number	200
Explicit Momentum Relaxation Factor	0.75
Explicit Pressure Relaxation Factor	0.75

Discretization Scheme

Variable	Scheme
Pressure	Standard
Momentum	First Order Upwind
Turbulent Kinetic Energy	First Order Upwind
Turbulent Dissipation Rate	First Order Upwind

Material Properties

Material: black-powder-magnetite (inert-particle)

Property	Units	Method	Value(s)
Density	kg/m ³	constant	5150
C _p (Specific Heat)	J/kg-K	constant	1680
Thermal Conductivity	W/m-K	constant	0.0454

Material: sales-gas (fluid)

Property	Units	Method	Value(s)
Density	kg/m ³	constant	61.799999
Cp (Specific Heat)	J/kg-K	constant	1006.43
Thermal Conductivity	W/m-K	constant	0.0242
Viscosity	kg/m-s	constant	1.33e-05
Molecular Weight	kg/Kmol	constant	28.966
Reference Temperature	K	constant	316

Material: steel (solid)

Property	Units	Method	Value(s)
Density	kg/m ³	constant	7833
Cp (Specific Heat)	J/kg-K	constant	871
Thermal Conductivity	W/m-K	constant	202.4

REFERENCES

- [1] Baldwin, R.M. "Black powder in the gas industry sources, characteristics and treatment" GMRC, Report No TA97-4, May1998
- [2] Baldwin, R.M. "Black powder control starts locally, works back to source" pipeline & gas industry, April 1999, pp.81-87
- [3] Baldwin, R.M. "Black powder problem will yield to understanding, planning" pipeline & gas industry, March 1999, pp.109-112
- [4] Tsochatzidis, N.A. and Maroullis, K.E.: "Methods help remove black powder from gas pipelines" Oil and gas journal, 2007, Vol.105, No. 10, pp. 52-58
- [5] Arrington, S "Pipeline debris removal requires extensive planning" pipeline & gas journal, November 2006, pp.61-62
- [6] Winters, R.H., "The black powder problem in gas pipelines," 2nd black powder forum, Lafayette, La., Nov. 1, 1999
- [7] T.S Vilela National institute of technology (INT), J.C. Cobucci Petrobras/cenpes/TMEC, Fernando Coelho TBG, Rio de Janeiro/RI-Brazil "Chemical and physical analysis of natural gas pipelines corrosion products (black powder)" 2002, Block 3-Forum 19 pp. 461-463

- [8] John Smart, Robert Winters., "Black powder migration in gas pipeline and associated problems" The pipeline pigging and integrity management conference. Feb.2008, Houston, Texas pp.3
- [9] Abdelmounam M.S, Saudi Aramco Journal of technology, Fall 2007 pp. 3-8
- [10] Gody, J.M., Carvalho, F., Cordilha, A., Matta, L.E. and Godoy, M.L.: "(210) pb content in natural Gas Pipeline Residues (Black powder) and its correlation with the chemical composition" Journal of environmental radioactivity, 2005, pp. 101-111
- [11] Sridhar, N. Dunn, D.S, Anderko, A.M, Lencka, M.M and schutt, H.U. "Effect of water and gas composition on the internal corrosion of gas pipelines-Modeling and Experimental studies" Corrosion Vol. 57, No.3, 2001, pp. 221-235
- [12] Craig, B. "Corrosion Product Analysis-A Road map to corrosion in oil and gas production" Material performance, August 2002, pp. 56-58
- [13] Lyle, F.F. "Carbon Dioxide/Hydrogen Sulfide Corrosion under wet low flow gas pipeline conditions in the presence of bicarbonate, chloride and Oxygen" PRCI final report PR-15-9313, 1997
- [14] John Smart "Movement of Black powder in gas pipeline by", John smart consulting Engineer Houston, Pipeline and Gas Journal, October 2007, pp. 82-85
- [15] "Transport of solids at low concentration in horizontal pipelines" in Advances in Solid-Liquid Flow in Pipelines and its Applications, Edited by Iraj Zandi, Pergammon Press, New York, 1971 pp. 101-124

- [16] Tsirkunov, Yuri, M., Volkov, Alekgei, N., Tarasova and Natalia, V., “Full Lagrangian approach to the calculation of dilute dispersed phase flows: advantages and applications” FED, ASME, 2002, Vol. 257 No. 2A, pp. 409-422
- [17] Crowe, C.T, Sommerfeld M, and Isuji, Y. “Multiphase flows with droplets and particles” CRC Press, 1998, pp. 92-93
- [18] Sommerfeld, M. “Analysis of collision effects turbulent gas-particle flow in a horizontal channel – part 1: particle transport”, *Int. J. Multiphase Flow*, 2003, Vol. 29 No.4, pp. 675-99
- [19] Lun, C.K.K., Liu, H.S., “Numerical simulation of dilute turbulent gas–solid flows in horizontal channels” *Int. J. Multiphase Flow*, 1997, pp. 575–605
- [20] Vance, M.W., Squires, K.D., Simonin O., “Properties of the particle velocity field in gas-solid turbulent channel flow”, *Physics of Fluids*; Jun 2006, Vol. 18 Issue 6, 2006
- [21] Durst, F.; Miloievic, D.; Schönung, B., “Eulerian and Lagrangian predictions of particulate two-phase flows: a numerical study”, *Applied Mathematical Modelling*, 1984, 8 (2), pp. 101-115
- [22] J.K. Keska, “Some experimental results of a transient and oscillatory flow pattern in gas solid flow” University of Nebraska-Lincoln, 1989, pp.31-39
- [23] Z. Li, Guangming Jiang, H. Henein and A. Vassilicos, “An experimental study of the dispersion of powders into a pipe turbulent gas stream” *Canadian institute of mining, metallurgy and petroleum*, 2000, Vol. 39, No 2, pp. 195-205

- [24] Daniel A. Khalitov, Ellen K. Longmire, "Effect of particle size on velocity correlations in turbulent channel flow" Proceeding of ASME FEDSM2003-45730, ASME_JSME Joint Fluids Engineering Conference, Honolulu, Hawaii, July 2003, pp. 445-453
- [25] Kulick, J.D., Fessler, J.R., and Eaton, J.K. "On the interactions between particles and turbulence in fully developed channel flow in air" Report MD-66, Stanford University, 1993
- [26] Michael J. Moran, Howard N. Shapiro, "Fundamentals of engineering thermodynamics" 5th Edition, 2004, pp. 119-121
- [27] Frank M. White, Fluid Mechanics, 6th Edition 2008, "Viscous flow in duct" pp. 356-362
- [28] Frank M. White, Fluid Mechanics, 6th Edition 2008, "Viscous flow in duct" pp. 363-365
- [29] Frank M. White, Fluid Mechanics, 6th Edition 2008, Conservation of Mass, pp.149-151
- [30] Frank M. White, Fluid Mechanics, 6th Edition 2008, Conservation of Mass, pp.353-356
- [31] J. Nikuradse, "Stromungsgesetze in Rauhen Rohren" VDI Forschungsh. English trans., NACA Tech. Mem. 2008, pp. 1933
- [32] R. V. Smith, Petroleum Consultant, Bartlesville, "Determining natural gas flow in pipe and annular conductors" section: Technology; Pipeline; Oil & Gas Journal pp. 119-129
- [33] Donald F. Young, Bruce R. Munson, Theodore H. Okiishi, "A brief introduction to fluid mechanics" 3rd Edition 2004 pp. 318-321

- [34] B. Johansson, C. Ljus, A. Almstedt, "Turbulence modification by particles in a horizontal pipe flow" *International journal of multiphase flow* 28, 2002, pp. 1075–1090
- [35] C.K.K. Lun, "Numerical simulation of dilute turbulent gas solid flows" *International journal of multiphase flow* 26, 2000, pp. 1707-1736
- [36] M. B. Staki, D. Z. Milojevi "The effect of particles on the gas velocity in a free turbulent flow". *Journal of engineering physics and thermo physics*, 1995, Vol. 68, No. 3, pp. 302-306